The medaka mutant deficient in *eyes shut homolog* exhibits opsin transport defects and enhanced autophagy in retinal photoreceptors

Keita Sato [1] · Yang Liu [2] · Takahiro Yamashita [3] · Hideyo Ohuchi [1]

1 Department of Cytology and Histology, Faculty of Medicine, Dentistry, and Pharmaceutical Sciences, Okayama University, Okayama 700-8558, Japan
2 Department of Cytology and Histology, Graduate School of Medicine, Dentistry, and Pharmaceutical Sciences, Okayama University, Okayama 700-8558, Japan
3 Department of Biophysics, Graduate School of Science, Kyoto University, Kyoto 606-8502, Japan

Correspondence should be addressed:
Keita Sato
keitasato@okayama-u.ac.jp
Hideyo Ohuchi
ohuchi-hideyo@okayama-u.ac.jp

Abstract

Eyes shut homolog (*EYS*) encodes a proteoglycan and the human mutation causes retinitis pigmentosa type 25 (RP25) with progressive retinal degeneration. RP25 most frequently affects autosomal recessive RP patients with many ethnic backgrounds. Although studies using RP models have facilitated the development of therapeutic medications, *Eys* has been lost in rodent model animals. Here we examined the roles for Eys in the maintenance of photoreceptor structure and function by generating *eys*-null medaka fish using the CRISPR–Cas9 system. Medaka EYS protein was present near the connecting cilium of wild-type photoreceptors, while it was absent from the $eys^{-/-}$ retina. The mutant larvae exhibited a reduced visual motor response compared with wild-type. In contrast to reported *eys*-deficient zebrafish at the similar stage, no retinal cell death was detected in the 8-month post-hatching (8-mph) medaka *eys*-mutant. Immunohistochemistry showed a significant reduction in the length of cone outer segments (OSs), retention of OS proteins in the inner segments of photoreceptors, abnormal filamentous actin network at the base of cone OSs in the mutant retina by 8 mph. Electron microscopy revealed aberrant structure of calyceal processes, numerous vesiculation and lamellar interruptions, and autophagosomes in the *eys*-mutant cone photoreceptors. In situ hybridization showed an autophagy component gene, *gabarap,* was ectopically expressed in the *eys*-null retina. These results suggest *eys* is required for regeneration of OS, especially of cone photoreceptors, and transport of OS proteins by regulating actin filaments. Enhanced autophagy may delay the progression of retinal degeneration when lacking EYS in the medaka retina.

Keywords ***eyes shut homolog*・*eys*・retinitis pigmentosa・RP25・cone photoreceptor・autophagy**

Introduction

Retinitis pigmentosa (RP) is the most common genetic disease of the retina, having a prevalence rate of approximately 1 in 5000 worldwide (Verbakel et al. 2018; O'Neal and Luther 2021). The initial symptoms are night blindness and peripheral vison loss, followed by gradual deterioration of visual acuity, loss of electroretinogram, and pigmentation of the ocular fundus called the bone spicule. More than 80 genes have been associated with RP, which can be inherited in an autosomal recessive (ar), autosomal dominant, X-linked, digenic, or mitochondrial manner.

The causal gene for RP type 25 (RP25) was identified by positional cloning (Abd El-Aziz et al. 2008; Collin et al. 2008) and found to be a human homologous gene for *Drosophila eye shut/spacemaker*, mutants of which lack the interrhabdominal space in the retina (Husain et al. 2006; Zelhof et al. 2006). Epidemiological data have shown that one of the most frequently encountered genes responsible for arRP is *EYS* in Japanese individuals (Hosono et al. 2012; Iwanami et al. 2012; Arai et al. 2015; Yang et al. 2020; Numa et al. 2020), as well as in East Asians and Europeans (Ruiz et al. 1998; Khaliq et al. 1999; Audo et al. 2010; Huang et al. 2010; Bandah-Rozenfeld et al. 2010; Di et al. 2016; Westin et al. 2021). The *Eys* gene encodes a secreted glycoprotein similar to proteoglycans of Agrin, Perlecan (heparan sulphate proteoglycan 2), Crumbs family member 1 (CRB1), and CRB2, consisting of a number of EGF-like domains and laminin globular domains (Haltom et al. 2014) and functioning as an extracellular matrix (ECM) protein (Husain et al. 2006; Zelhof et al. 2006).

In human and other vertebrate retinas, there are photoreceptor cells called rods and cones. The outer segment of photoreceptors is an altered structure of the apical, ciliary portion of the cell, forming a stack of disks that are penetrated by opsin photopigments. The inner segment of photoreceptors is located between the outer segment and cell nucleus and is densely packed with mitochondria. It has been shown that EYS protein is localized to the outer segment of photoreceptors and at the boundary region between the inner and outer segments in pig, macaque, and human retina (Abd El-Aziz et al. 2008; Yu et al. 2016).

The pathophysiology underlying RP is mostly assumed to be degeneration and ultimate cell death of photoreceptor cells due to mutations of the genes encoding molecules specifically functioning in the rod/cone photoreceptors, retinal pigment epithelial cells (RPE), or Muller glial cells (for review; Newton and Megaw, 2020; Wright et al., 2010). Although palliative treatments such as vitamin A-related, neuroprotective, and circulation-improving drugs have been widely advocated, there are increasing demands for developing novel therapies based on gene- and mutation-specific investigations. No

fundamental remedies, however, have been made based on studies on the pathogenesis of *Eys* mutations.

Since mice do not have the *Eys* gene (Abd El-Aziz et al. 2008), we generated a homozygous mutant medaka, *Oryzias latipes,* with a loss of function of the *eys* gene. The medaka fish has been utilized as an experimental model animal (Wittbrodt et al. 2002). Medaka is a distantly related teleost to zebrafish, *Danio rerio*, sharing its last common ancestor with zebrafish between 200 and 300 million years ago (Schartl et al. 2013). The whole genome was duplicated in the common ancestor, and medaka and zebrafish underwent independent evolution of the duplicated genes, resulting in different biology due to divergent usage or deletion of duplicated genes.

We found that the *eys*$^{-/-}$ medaka fry exhibited a reduced visual motor response (VMR) immediately after hatching. The matured *eys*$^{-/-}$ retina showed retention of outer segment (OS) proteins in the inner segments of photoreceptors. The length of cone OSs was significantly reduced in the *eys*-deficient retina, while the thickness of rod OSs was not altered. In contrast to the reported zebrafish *eys* mutants, retinal cell death was not detected in the medaka *eys* mutant examined. Instead, the expression of a macroautophagy (autophagy)-related gene was ectopically induced in the outer nuclear layer where the nuclei of photoreceptor cells reside. Since retinal regenerative capacities are limited in medaka compared with zebrafish (Lust and Wittbrodt 2018), these results imply a different mechanism to maintain retinal integrity by escaping retinal cell death in medaka retina as a translational potential.

Results

Generation of *eys*$^{-/-}$ medaka

Numerous mutations in the human *EYS* gene have been found, and the pathophysiology of each mutation may be different, depending on the domains of the protein affected by the mutation and the types of mutations, such as missense and nonsense mutations. To examine the role of *eys* in photoreceptor maintenance, we sought to generate a null mutation of medaka *eys* using the CRISPR–Cas9 system. According to the public database (Ensembl), the predicted medaka EYS protein has 3018 amino acids, consisting of a signal peptide, 41 EGF domains/calcium binding EGF domains, and 5 laminin G domains in the C-terminal region (Fig. 1c). Likewise, the medaka *eys* gene is considered to comprise 51 exons, spanning 206 kb on chromosome 15 (Fig. 1d). In fact, we isolated several medaka *eys* cDNA clones ranging from full-length to shorter isoforms and confirmed *eys* expression in the medaka eye (Fig. 1a, b). Based on the *eys* genomic structure, we selected two target sequences for genome editing with the CRISPR–Cas9 system: one in intron 1 (target 1), and the other in the coding sequence of exon 2 (target 2) (Fig. 1e). By injecting a mixture of the two sgRNAs and Cas9 protein, we obtained F0 medaka larvae containing *eys*-deleted cells, and the *eys* mutations were subsequently transmitted to the germline. Finally, we established a homozygous 930-bp deletion mutant of the *eys* gene (Fig. 1f, g). We also verified that exon 2 was deleted in the transcripts of *eys*$^{-/-}$ fish (Fig. 1h, i). Exon 2 normally encodes 830 nucleotides, including the initiation codon, and skipping this exon by genome editing resulted in no expression of the EYS protein (Fig. 3c, Fig. 3b as a control). We could not find obvious differences between WT and *eys*$^{-/-}$ medakas in general appearance including eye morphology, body length, swimming behaviour, and feeding behaviour.

Visual motor response (VMR) showed defects in *eys*-mutant medaka immediately after hatching

To evaluate the visual functions of *eys*$^{-/-}$ medaka as early as possible, we measured the VMR of the fry at one to two days post-hatching (1-2 dph) and compared it with that of the wild-type. VMR is an assay that captures the startle response to sudden changes in the light environment (dark to light, light-on response; light to dark, light-off response) as changes in locomotion and speed (Emran et al. 2008). Individual movements of the fry were recorded as images in a 48-well dish, and digitalized data were analysed. In light-on response experiments, wild-type fry exhibited a slow response at the peak of 15 seconds after light stimulation, while the response was significantly reduced in the case of *eys*$^{-/-}$ fry (Fig. 2a, Fig. S3a, b). In light-off response experiments, wild-type fry

exhibited an immediate response at the onset of dark and a subsequent continued response, while the later response was significantly reduced in *eys*$^{-/-}$ fry (Fig. 2a, Fig. S3b). Tracking data for the fry in the light-off response showed obviously decreased locomotion in the *eys*$^{-/-}$ mutant (Supplementary Movies 1, 2). These results suggested that in the absence of EYS, the fast startle response to changes in lightening was maintained, but the later slow responses were substantially disturbed, which was more obvious in a light to dark environment (light-off response). As we hypothesized that developmental delay in the retinal photoreceptors might underly defects of VMR in the *eys*$^{-/-}$ larva, the retina was immunostained with anti-visual pigment antibodies after verification by Western blot analysis (Fig. S2). We found that all *eys*$^{-/-}$ retina examined (n = 4) exhibited retention of photopigments except for UV opsin, mainly in the ventral region, but most of wild-type retina did not (Fig. 2b-s, Fig. S4). In the *eys*$^{-/-}$ cones which exhibited retention of photopigment proteins, formation of the outer segments was delayed (Fig. S4d-f; Fig. S4a-c as control).

Localization of EYS protein in medaka retina

To reveal the localization of EYS, we performed immunostaining using an antibody against a portion of human EYS (Fig. S1). We used an anti-EYS antibody that was developed against 66 amino acids of human EYS protein for EGF domains (open triangle in Fig. 1c; Fig. S1). The amino acid identity/similarity between medaka and human EYS was 56.7/68.7%, which might miss detection of a lower amount of medaka EYS in the retina (El-Aziz et al., 2008; Lu et al., 2016). EYS immunoreactivity exhibited a punctate pattern in wild-type retina, which is similar to that reported for zebrafish (Fig. 3a, b). Since these punctate fluorescent signals were not detected in *eys*$^{-/-}$ retina (Fig. 3c), we concluded that this anti-EYS antibody could detect medaka EYS protein. We next examined whether EYS protein was present in rods and/or cones. Coimmunostaining with the antibody against each photopigment and anti-EYS antibody showed that EYS was present at the base of UV-, green-, and red-cone OSs as well as rod OSs (Fig. 3d-g). EYS proteins were localized to the basal end of acetylated α-tubulin, a molecular marker for the ciliary microtubule axoneme (Fig. 3h, i). Higher magnification confocal microscopy images revealed EYS immunoreactivity of two to three short fibre-like, separate structures in the connecting cilium (CC) of photoreceptors (Supplementary Movies 3 and 4). Thus, we concluded that EYS was localized to the basal end of the CC of *all* types of photoreceptors in medaka retina.

No histological evidence of cell death in 8-mph *eys*$^{-/-}$ retina

Zebrafish *eys*$^{-/-}$ retina was reported to exhibit loss of photoreceptors at 6 months post-fertilization (6 mpf) (Yu et al. 2016). We therefore examined the histology of medaka *eys*$^{-/-}$ retinas at 8 mph with hematoxylin and eosin (HE) staining to observe cell death in the *eys*-mutant retina (Fig. S5a, b). However, at this stage, medaka *eys*$^{-/-}$ retinas did not show obvious morphological differences compared with wild-type retinas at the same stage.

We next quantified the thickness, number, and average length of the wild-type and *eys*$^{-/-}$ photoreceptor outer segments at 8 mph. We identified rod and cone photoreceptors by immunolabelling with anti-photopigment antibodies (Fig. S5c-j). We first measured the thickness of rod outer segments (ROS) layer in the dorsal and ventral retina from wild-type and *eys*$^{-/-}$ medaka (Fig. S5c, d). We found that there was no significant change in the thickness of ROS layer between the two genotypes (Fig. 4a). Regarding the cone opsin outer segment (COS), we measured the number of each COS per unit area (Fig. S5k-m) and the average length of each COS (Fig. 4b-d). The number of COS was not significantly different between the two genotypes, while the average length of all types of COS was significantly reduced in the *eys*$^{-/-}$ ventral retina compared with wild-type. The length of red COS was also significantly reduced in the *eys*$^{-/-}$ dorsal retina (Fig. 4d).

These data suggested that at 8 mph, there was no significant change in the number of photoreceptors between the two genotypes and that cone-dominant reduction in the OSs was observed in the *eys*-deficient retina, more evidently in the ventral retina. Consistent with this observation, we could not detect TUNEL-positive cells in *eys*$^{-/-}$ or wild-type retinas at 8 mph, while numerous TUNEL-positive cells were detected in the retina after treatment with ouabain, a Na+/K+ ATPase inhibitor used as a cell death inducer (Fimbel et al. 2007) (not shown). Immunohistochemistry for cleaved caspase 3 did not reveal any positive cells in the 8-mph mutant retina, either (not shown).

Retention of outer segment proteins in *eys*$^{-/-}$ photoreceptors

Photoreceptor outer segments (OSs) regenerate daily, and nascent disks are formed at the base of OSs through the incorporation of molecules transported from the inner segment (Hsu et al. 2015; Barnes et al. 2021). Because medaka EYS was present in the vicinity of CC, we sought to examine whether EYS was involved in the transport of proteins to the OS. We visualized each medaka opsin as well as peripherin 2 (Prph2) by immunostaining. Normally, these proteins are transported to photoreceptor disks for their maintenance. Prph2 is a tetraspanning protein localized to the disk rims of all photoreceptors, while opsin pigments reside in the ciliary plasma membrane, OS plasma membrane, and OS disk lamellar membrane (a review, Goldberg et al., 2016). We found that these OS proteins were mislocalized in a subset of cells of the *eys*$^{-/-}$ retina (8 mph) (Fig. 5). In

contrast to wild-type (Fig. 5a, e, i, m), in the mutant retina (Fig. 5b, c, f, g, j, k, n, o), the OS proteins remained in the inner segment, cell body, or even in the basal processes, synaptic region of photoreceptors (arrowheads in Fig. 5). Most likely due to the difference in localization within the disk, retention of photopigments was more evident than that of Prph2 (Fig. 5g, k, o). We therefore focused on opsins to quantify the number of cells that exhibited their retention in the inner segments or even in the cone pedicle (Fig. 5d, h, l, p). In the *eys*$^{-/-}$ retina, the number of photoreceptors that impaired the transport of these photopigments was significantly increased. Thus, we concluded that EYS was required for the proper transport of these OS-resident molecules.

Filamentous actin network and calyceal processes are deteriorated in *eys*$^{-/-}$ cone photoreceptors

Medaka EYS protein is present near the CC, the OS base where the biogenesis of the disks is initiated. Recent studies have revealed that the filamentous actin (F-actin) network is crucial in this process (Spencer et al. 2019; Corral-Serrano et al. 2020). We therefore examined whether the absence of EYS influenced the F-actin structure of this region. Since *eys*-null medaka exhibited cone-dominant defects, as shown, we focused on cone photoreceptors. Double staining for phalloidin and cone photopigments revealed a transverse line of ciliary stalk F-actin (Schietroma et al. 2017) residing at the base of each photoreceptor OS in *eys*$^{-/-}$ as well as in wild-type (arrowheads in Fig. S6i-l). Thus, F-actin seemed to localize at the site of initiation of new disk (lamella) formation even in the absence of EYS. In contrast, actin filaments axially oriented in *eys*$^{-/-}$ cones were scarcer, and their arrays were irregular and randomized compared with those of wild-type cones (Fig. 6b, S6f, S6h; Fig. 6a, S6e, S6g as controls). This finding appeared to correlate to F-actin bundles of the calyceal processes, which are axially oriented microvilli protruding from the apical region of the inner segment, forming a collar around the base of the OS (Brown et al. 1963; Sahly et al. 2012) (Fig. S6a, b). It is known that humans, macaques, pigs, *Xenopus*, and teleosts have this structure, while mouse photoreceptors lack calyceal processes (Kusmic et al. 1993; Sahly et al. 2012). We hypothesized that EYS might be required for the maintenance of calyceal processes in medaka photoreceptors. To test this, we employed scanning electron microscopy (SEM) and found that in wild-type cones, microvilli for calyceal processes were regularly aligned, and the distance between the microvilli appeared to be constant (Fig. S6c, d; Fig. 6c, d, g-j), whereas those of *eys*$^{-/-}$ cones were deteriorated, and the microvilli were aberrantly aligned (Fig. 6e, f, k-n). Thus, we concluded that the absence of EYS protein led to morphological deterioration of the calyceal processes and that EYS was required for their maintenance.

Ultrastructure of cone outer segments shows regeneration defects in the *eys*$^{-/-}$

We further examined the ultrastructure of cone photoreceptors, especially focusing on the CC and its surrounding tissues, and compared them between wild-type and *eys*-null medaka. By transmission electron microscopy (TEM), we first identified ciliary pockets in the wild-type medaka cone photoreceptors at 5 mph (Fig. 7a, b). In the *eys*-mutant, there were varying degrees of morphological changes. In almost normal-appearing cones (Fig. 7c-g), we identified ciliary pockets (Fig. 7d). Higher magnification TEM images showed vesiculation at the base of OS abutting the inner segment (Fig. 7e) or at the disk edge of the distal region (Fig. 7g) and an interrupted lamellar membrane (Fig. 7f). These small vesicles and the occasional lamellar interruptions in the OS were also found in some wild-type cones (Fig. 7a). However, in the *eys*-mutant, more obvious morphological alterations were observed (Fig. 7h): larger vesicles or loops at the disk edges (Fig. 7i) and numerous small vesicles in the accessory outer segments (AOS) (Fig. 7j), which were not observed in the wild-type AOS (Fig. 7a, b) and in those of normal-appearing cones (Fig. 7c, d). In the most severely affected cones, numerous small vesicles and loops were observed in the OS, and fragmented disk-stacking of OS was observed (Fig. 7k, l). Based on these TEM observations, we classified the morphological phenotypes of cone photoreceptors in the wild-type and *eys*-deficient retinas into three categories, finding that *eys*-deficient cone photoreceptors were significantly disrupted compared with wild-type photoreceptors (Fig. 7m). These data showed that EYS was indispensable for the maintenance of cone photoreceptors, especially for the morphological integrity of their OSs.

Decreased expression of photoreceptor-specific/*eys*-related genes verifies retinal defects in the *eys*-deficient retina

To support the above morphological changes in the *eys*-null retina, we examined the mRNA expression levels of each photoreceptor-specific phototransduction cascade gene (Larhammar et al. 2009), such as *gnat, pde6,* and *grk* using the primers listed in Table S3 (Fig. S7a). Accordingly, the expression levels of *grk1a*, a rod-specific gene, and *pde6c*, a cone-specific gene, were significantly decreased in the *eys*$^{-/-}$ retina at 8 mph compared with the wild-type retina. These results implied that even without an obvious morphological deterioration of rod photoreceptors by 8 mph, a functional decline in G protein-coupled receptor kinase activity was emerging in the *eys*-deficient retina.

We further examined the mRNA expression levels of known EYS-related molecules and EYS-interacting proteins to determine the effects of the absence of *eys* expression in

the retina (Fig. S7b, Table S3). As mentioned, EYS consists of repeated EGF and laminin G domains (Fig. 1c). Structurally similar proteins include agrin, heparan sulphate proteoglycan 2, and EGF-like fibronectin type III laminin G domains encoded by *agrn*, *hspg2*, and *egflam*, respectively. We also examined *crumb* (*crb*) homologues, which encode a transmembrane protein, partly resembling EYS. qPCR analysis showed that the relative mRNA levels of *agrn* and *crb1a* were significantly decreased compared with those of wild type (Fig. S7b). Regarding EYS-interacting proteins, we examined the expression of Prominins, a possible transient interaction partner of EYS. There are three *prominin* homologues, *prom1a*, *prom1b*, and *prom2* in medaka. None of these *prom* genes exhibited significantly altered expression in the *eys*-mutant retina compared with the wild-type retina, (Fig. S7b). Thus, the gene expression of *eys*-related genes, encoding proteoglycans, was not upregulated to compensate for the absence of EYS; instead, decreased expression of *grk1a, pde6c, agrn,* and *crb1a* verified a certain degree of defects in photoreceptors of *eys*$^{-/-}$ medaka at 8 mph.

The expression of an autophagy-related gene is ectopically induced in *eys*-null photoreceptors

Since we could not histologically detect obvious cell death, we tested the mRNA expression levels of oxidative stress-responsive genes and apoptosis- or autophagy-related genes (Fig. S7c, d, Table S3). Excluding a significant downregulation of *sod1* (*superoxide dismutase 1*), the genes examined showed significant alterations in their expression levels in *eys*-deficient whole retinas at 8 mph compared with wild-type retinas. We next determined the mRNA localization of *bax* (*bcl-2-associated x*) (proapoptotic), *bcl2* (*b-cell lymphoma 2*) (anti-apoptotic), *mlkl* (*mixed lineage kinase domain like*) (necroptosis), and *gabarap* (*gaba type a receptor-associated protein*) (autophagy)(for review, Nakamura and Yoshimori, 2017; Schaaf et al., 2016; Yamamoto and Mizushima, 2021) in the 4 mph retina of *eys*$^{-/-}$ and wild-type fishes by in situ hybridization (Fig. 8a-d, S8). Interestingly, we found that a considerable amount of mRNA expression for these genes was diffusely observed even in the wild-type retina at this stage, indicating that remodelling of retinal cells occurs in the normal medaka (Fig. S8a, b for *bax*). Additionally, the expression of *gabarap* was ectopically induced in the outer nuclear layer, where photoreceptor cell nuclei are localized, only in the *eys*-mutant medaka (Fig. 8a, b). Furthermore, TEM revealed many double-membraned structures and autophagosomes in the inner segments of *eys*-deficient photoreceptors (Fig. 8f, h), while no such organelles were detected in wild-type photoreceptors (Fig. 8e, g). These data suggested that the autophagy system was likely to be activated in the photoreceptors of *eys*-deficient retinas.

Discussion

This study shows medaka EYS protein is localized near the connecting cilia (CC) (Fig. 9). In *eys*$^{-/-}$ cone photoreceptors, protein transport to the outer segment (OS) is impaired, actin filament networks and calyceal processes are disorganized, and ultrastructure of the OS is disturbed, leading to reduced expression of phototransduction cascade genes and upregulation of autophagy-related genes. By eliminating OS proteins that have accumulated due to the protein transport defects, autophagy is thought to alleviate cellular stress and prevent cell death.

To elucidate the pathogenesis of retinal degeneration caused by *EYS* mutations, we used medaka, an experimental model fish that is evolutionally distant from zebrafish. Our *eys*$^{-/-}$ medaka mutant and zebrafish (Yu et al. 2016; Lu et al. 2017; Messchaert et al. 2018) exhibit cone dominant phenotypes, while human *EYS*-mutated patients not often display cone-rod dystrophy (Katagiri et al. 2014; Pierrache et al. 2019). There are several explanations for this. Immunohistochemistry has shown that EYS localizes to the OSs of rods and cones in the primate retina (Abd El-Aziz et al. 2008; Yu et al. 2016), while EYS is detected only in the CC region of both photoreceptors in fish. The difference in the localization of EYS may reflect functional differences in EYS in mammals and fish. Another possibility is that loss-of-function mutations in the *EYS* gene may primarily result in cone dominant phenotypes and that neomorphic mutations in EYS may lead to rod dominant phenotypes. Numerous types of human *EYS* mutations have been reported: for example, a hypomorphic variant was recently reported (Garcia-Delgado et al., 2021, for a review; Nishiguchi et al., 2021). Thus, the pathogenesis of RP25 seems to be multifaceted, including defects in interactions with other extracellular substrates by a shortened EYS. Also, since identical genotypes can cause both RP and cone-rod dystrophy in the case of human patients, the presence of certain modifier genes has been postulated (Katagiri et al. 2014; Pierrache et al. 2019). The *eys*-null medaka that we have developed does not express EYS protein in the retina due to disruption of the start codon. This medaka will help to identify interacting molecules of EYS that are crucial to the identification of certain medical interventions for *eys*-associated disease.

The *Drosophila* orthologue of EYS, eyes shut/spacemaker, is an interrhabdomeral secreted protein, and also localizes to the cell surface when cotransfected with prominin (Prom) (Zelhof et al. 2006; Nie et al. 2012). Thus, Prom is regarded as a possible transient interaction partner for EYS. In *Xenopus*, the *Prom1*-null mutant exhibits severe dysmorphic cone photoreceptors (Carr et al. 2021). *Xenopus* Prom1 is more predominantly localized to cone OS (COS) than rod OS (ROS) (Han et al. 2012). This localization pattern of Prom1, if true in fish, may explain why *eys*-null fish show a cone-

dominant phenotype. Consistently, in the zebrafish *prom1b*-null mutant, cones degenerate earlier than rods (Lu et al. 2019). Thus, interaction with PROM may also relate to a cone-dominant role of EYS in fish.

The visual motor response (VMR) to light-on and light-off stimulations as early as 1 to 2 dph was significantly impaired in the mutant larva, reflecting its developmental delay in the ventral retina. VMR has been used to evaluate visual functions in zebrafish exhibiting retinal degeneration (Zhang et al. 2016; for a review, Ganzen et al. 2017). It has been reported that a zebrafish *eys*-mutant exhibits reduced VMR in the light-on response (Messchaert et al. 2018). They focused on the light-on response because the light-off response in zebrafish is driven not only by retinal photoreceptors but also by brain photoreceptors (Fernandes et al. 2012; Ganzen et al. 2017). We showed that the transition from dark to light did not induce an immediate response but a slow, transient increase in activity over approximately 15 seconds in wild-type medaka. The light-off response was more immediate and greater than the light-on response and showed sustained activity. These VMR response patterns in medaka differ from those of zebrafish, which show a clear activity peak immediately at the time of light-on and -off (Carter et al., 2020; Liu et al., 2015; Messchaert et al., 2018). Although these differences should be further pursued using the same platform, the VMR is useful to detect and screen visual defects for larval medaka.

We identified finer images of medaka EYS protein showing two to three short fibre-like, separate structures in the CC resembling transition zone proteins as recently reported (Shi et al. 2017). The CC region of PRs includes the machinery for protein transport to the outer segment, which is indispensable for the daily renewal of outer segment disks (for review, Barnes et al., 2021). Retention of OS proteins in *eys*$^{-/-}$ medaka retina suggests crucial roles for EYS in this system. It is thus reasonable to observe degenerating cone OSs as revealed by electron microscopy in this region of *eys*-deficient retina, leading to decreased transcription of PR/*eys*-related genes. The significant reduction in cone OS length in the ventral retina is likely due to a greater level of external light from the overhead direction (Zhang et al. 2008).

It has been shown that calyceal processes control the sizing of rod disks and cone lamellae throughout their daily renewal in *Xenopus* (Schietroma et al. 2017). Our study showed that calyceal process F-actin was reduced and misaligned in the absence of EYS. Thus, medaka EYS in the CC region likely plays a role in regulating OS daily renewal by preserving the integrity of calyceal processes. Since calyceal processes are surrounded by ECM and secreted EYS likely occupies their extracellular space, it is conceivable that EYS nourishes the calyceal processes. Prom was originally found to be present in

microvilli of epithelial cells and plasma membrane protrusions of nonepithelial cells (Weigmann et al. 1997). A recent study showed that a component of calyceal processes is located in a position external to Prom1 in the macaque retina (Verschueren et al. 2022). Thus, medaka EYS may maintain the calyceal processes via Prom1.

PR cell death could not be histologically identified in this study at 8 mph. Instead, the *eys* mutant showed upregulation of *gabarap* in the outer nuclear layer. GABARAP belongs to the ATG8 family, autophagy-related ubiquitin-like proteins consisting of 8 members in medaka. Autophagy (macroautophagy) is an evolutionally conserved cytoplasmic degradation system in which cytoplasmic materials are sequestered by double-membraned vesicles and autophagosomes, and then fused to lysosomes for degradation (for review, Nakamura et al., 2022). The autophagy system is accelerated in the photoreceptor cells of *eys*$^{-/-}$ medaka, as we observed autophagosomes by TEM only in the mutant retina. Since ATG8 family proteins remains associated with autophagosomes, they have been utilized to monitor the formation of autophagosomes (Kabeya et al. 2004). Recent studies have revealed that there are differences in localization and functions among each ATG8 family protein, having functions of related and unrelated to autophagy (for review, Nakamura et al., 2022; Schaaf et al., 2016). Our study showed that all of ATG8 family members were transcribed in the adult medaka retina and eye, suggesting their roles in the medaka normal retina and in its pathological conditions.

In the eye, autophagy is involved in light-induced degradation of misfolded proteins, which prevents PR cell death in normal retinas (Chen et al. 2013; Wen et al. 2019) and regulates the F-actin network (Tang et al. 2013; Yamamoto et al. 2021). The activated autophagy system in *eys*$^{-/-}$ medaka retina may ameliorate PR degeneration and delay PR death. Medaka retina displays limited regenerative potential after retinal injury compared with zebrafish (Lust and Wittbrodt 2018). Hence, the medaka retina may have a very different system to escape or delay retinal cell death, such as augmentation of the autophagy system to support photoreceptor survival, which should be examined in detail in a subsequent study.

Materials and methods

Animals

The medaka fish (*Oryzias latipes*) strain d-rR was maintained and bred at Okayama University. The fish were kept under a light/dark cycle of 14/10 h at 26 ± 1 °C. Sexually mature fish in the light period, 4–10 h after light-on, were used for histological analysis. The light intensity was 2000 lux. The average body lengths of the WT and *eys*$^{-/-}$ fish used were 2.84 ± 0.19 mm (mean ± standard deviation (s.d.), n = 18) and 2.73 ± 0.20 mm (mean ± s.d., n = 24), respectively, which were not significantly different (P=0.083, unpaired two-tailed Student's t test). The fish were euthanized using 0.04% tricaine methanesulfonate and immediately decapitated thereafter. The use of animals in these experiments was in accordance with guidelines established by the Ministry of Education, Culture, Sports, Science and Technology of Japan.

Synthesis of single-guide RNA

Target sites for genome editing were chosen using the web tool CRISPRdirect (https://crispr.dbcls.jp/) to minimize the possibility of off-site cleavage (Naito et al. 2015). The 12-mer nucleotides in the 3′ region, adjacent to the PAM, of the two chosen target sequences were only found at the on-target sites in the medaka genome. Single-guide RNAs (sgRNAs) were synthesized as follows. First, PCR was performed using the DNA oligo containing the T7 promoter sequence, the 20-base target sequence, and the 5'-edge of the sgRNA scaffold and reverse complement primer of the 3'-side of the sgRNA scaffold using the DNA oligo of the sgRNA scaffold sequence as a template. The PCR product was purified by ethanol precipitation with ammonium acetate. Transcription of the sgRNAs was performed using Thermo T7 polymerase (TOYOBO, #TRL-201). The synthesized sgRNA was purified by ethanol precipitation with ammonium acetate. The precipitated RNA was finally dissolved in nuclease-free duplex buffer (Integrated DNA Technologies, #11-01-03-01). The oligo sequences used for sgRNA synthesis are listed in Table S2.

Microinjections

Fertilized medaka eggs were collected after natural spawning. Embryos at the one- or two-cell stage were injected with the mixture (21.9 μM of sgRNA for target1, 18.2 μM sgRNA for target2, 5.4 μM SpCas9 protein, 0.05% phenol red) using an Eppendorf microinjector 5242. The injection volume was adjusted to be comparable to the apparent size of the oil droplets.

Genotyping and RNA expression analysis

Genomic DNA was extracted from embryos at 4-6 dpf or caudal fin tissue from adult medaka. The egg chorion was broken by the micropipette tip end. The tissue was incubated in 50 µl of 50 mM NaOH at 95 °C for 10 minutes and neutralized by the addition of Tris-HCl. Then, 0.5 µl of the lysed samples was used as the PCR template. One microlitre each of 2 µM forward and reverse primers (see Table S2) and 2.5 µl of EmeraldAmp Max PCR Master Mix (Takara, RR320A) were combined. Samples were denatured at 95 °C for 3 minutes followed by 35 cycles of amplification consisting of 30 seconds each at 95, 60 and 72 °C. The samples were separated by agarose gel electrophoresis. To examine the edited genomic sequence, PCR products were sequenced directly.

To examine mRNA transcribed from the edited *eys* genomic locus, total RNA was extracted from the eye by NucleoZOL (Macherey-Nagel, # 740404.200) according to the manufacturer's instructions. Genomic DNA was removed using the AccuRT Genomic DNA Removal Kit (Applied Biological Materials, #G488). Total RNA was denatured by heating at 65 °C for 5 minutes followed by quick cooling on ice in the presence of random primer dN_{15}. Reverse transcription was performed at 30 °C for 10 minutes and 42 °C for 60 minutes with 2 µM random primer dN_{15}, 0.32 µg/µL MMLV RT, 1.6 U/µL RNase inhibitor (Takara, #2313A), 1 mM dNTP mix (NEB, #N0447S), 50 mM Tris-HCl (pH 8.0), 75 mM KCl, 8 mM $MgCl_2$, and 10 mM DTT. After the reaction, MMLV RT was denatured by heating at 95 °C for 5 minutes. The RT minus control was prepared as described above by omitting MMLV RT from the reaction. A total of 0.5 µl of 10-fold diluted reaction mixture was used as the PCR template. One microlitre each of 2 µM forward and reverse primers (see Table S2) and 2.5 µl PrimeSTAR Max PCR Master Mix (Takara, #R045A) were mixed. Samples were amplified by 35 cycles of 10 seconds at 98 °C, 5 seconds at 60 °C and 5 seconds at 72 °C. The samples were separated by agarose gel electrophoresis. PCR products were ligated into EcoRV-digested pBluescript II KS+ (Staratagene). After colony-directed PCR was performed with T7 and T3 primers, the PCR product was sequenced. To alleviate off-target defects, backcrossing the G0 mutant to WT was once performed.

Identification of the full-length coding region of medaka *eys*

The first-strand cDNA was prepared using the same method as that used to examine mRNA transcribed from the edited *eys* genomic locus, except that $dT_{23}VN$ was used as a primer and that 10 minutes of incubation at 30 °C was omitted. A total of 1 µl of 10-fold diluted RT reaction mixture was used as the PCR template. The PCR mixture contained

0.4 U KOD FX Neo polymerase (TOYOBO, #KFX-201), 1x PCR Buffer for KOD FX Neo, 0.4 mM (each) dNTP mix, and 0.25 μM each of forward and reverse primers. Samples were amplified by a single denaturing step of 2 minutes at 94 °C and 35 cycles of 10 seconds at 98 °C and 330 seconds at 68 °C. The samples were separated by agarose gel electrophoresis. After gel extraction of the 8-10-kb region, it was used as a template for nested PCR. The PCR conditions for nested PCR were the same as those for the 1st PCR except for the template and primers. The nested PCR samples were purified by a FastGene Gel/PCR Extraction Kit (Nippon genetics, FG-91302), digested with NotI, and ligated to the pJAZZ OC NotI vector using the BigEasy v2.0 Linear Cloning System (Lucigen, #43024-1). Colonies were picked and cultured in LB medium. Cells were collected by centrifugation, and plasmids were extracted using a FastGene Plasmid Mini Kit (Nippon gene, FG-90502). The presence or absence of the insert was confirmed by electrophoresis of NotI-digested plasmids. The isolated full-length coding region of *eys* cDNA was sequenced using the primers listed in Table S2.

Immunofluorescence

After the eyes were dissected from adult medaka, they were fixed overnight in 4% paraformaldehyde (PFA) in phosphate-buffered saline (PBS) at 4 °C. The tissues were subsequently immersed in 20% sucrose in PBS overnight for cryoprotection and were frozen in OCT compound (Tissue Tek; Sakura Finetek, Tokyo, Japan) in a deep freezer at −80 °C. Frozen tissues were sliced into 16-μm sections and attached to glass slides (CREST-coated glass slide; Matsunami Glass, Osaka, Japan). These glass slides were stored at −20 °C until use. For better visualization of the photoreceptor outer segment by bleaching melanin, the sections were irradiated with white light (50000 lux) in 0.3% H_2O_2, 40% methanol, and 60% PBS at RT for 12 hours (Korytowski and Sarna 1990) except for the case of phalloidin staining, which is incompatible with this bleaching procedure. This procedure also removes endogenous peroxidase activity. The sections were blocked with 1% bovine serum albumin (BSA) in PBS containing 0.1% Triton X-100 (PBSTx) at RT for 30 minutes in a humidified chamber. The following primary antibodies were diluted with IMMUNO SHOT immunostaining-Fine (Cosmo Bio) and applied to slides overnight at 4 °C. After washing with PBSTx, the slides were incubated with the appropriate secondary antibodies diluted with PBSTx containing 1% BSA for 1 hour at RT in a humidified chamber. F-actin was stained with 1.67 ug/ml TRITC-phalloidin (Fluka, 77418). For visualization of the nuclei, the sections were counterstained with 1 μg/ml Hoechst 33342. After washing with PBSTx three times, the

sections were coverslipped with VECTASHIELD Vibrance Antifade mounting medium (Vector Laboratories, H-1700) for phalloidin staining or with homemade mounting medium containing polyvinyl alcohol and glycerol for others. The antibodies used in this study and the dilution factors are summarized in Table S1.

Confocal fluorescence microscopy

Confocal fluorescence images excluding those shown in Figure 3h and i were collected with a Carl Zeiss LSM 780 laser scanning confocal microscope system with 405, 488, and 561-nm laser lines. Figure 3h and i were imaged on a Leica Stellaris 8 confocal microscope and were processed with Leica LIGHTNING deconvolution software. Brightness and contrast adjustments were performed for some images, and image manipulation was performed using a ZEN 2012 SP1 black edition or Leica Application Suite X 4.2.1.23810. Confocal z-stack images were acquired at 0.660-µm intervals for a total depth of 8.58 µm (Fig. 2b, i, k), at 0.660-µm intervals for a total depth of 7.26 µm (Fig. 2c), at 0.660-µm intervals for a total depth of 6.60 µm (Fig. 2d, j), at 0.647-µm intervals for a total depth of 7.77 µm (Fig. 2e), at 0.540-µm intervals for a total depth of 9.72 µm (Fig. 2f-h), at 0.647-µm intervals for a total depth of 5.83 µm (Fig. 2l), at 0.540-µm intervals for a total depth of 8.64 µm (Fig. 2m), at 0.540-µm intervals for a total depth of 8.10 µm (Fig. 2n), at 0.554-µm intervals for a total depth of 10.53 µm (Fig. 2o), at 0.660-µm intervals for a total depth of 5.28 µm (Fig. 3a), at 0.525-µm intervals for a total depth of 8.41 µm (Fig. 3b), at 0.525-µm intervals for a total depth of 6.31 µm (Fig. 3c), at 0.638-µm intervals for a total depth of 5.74 µm (Fig. 5a), at 0.638-µm intervals for a total depth of 7.66 µm (Fig. 5b), at 0.547-µm intervals for a total depth of 10.94 µm (Fig. 5e), at 0.525-µm intervals for a total depth of 8.93 µm (Fig. 5f), at 0.638-µm intervals for a total depth of 7.65 µm (Fig. 5i), at 0.525-µm intervals for a total depth of 6.31 µm (Fig. 5j), at 0.638-µm intervals for a total depth of 8.29 µm (Fig. 5m), at 0.647-µm intervals for a total depth of 11.01 µm (Fig. 5n), at 0.530-µm intervals for a total depth of 11.13 µm (Fig. 6a), or at 0.530-µm intervals for a total depth of 9.54 µm (Fig. 6b).

Scanning electron microscopy

For scanning electron microscopy (Hodel et al. 2014), the dissected eyes were fixed overnight in 2% PFA and 2% glutaraldehyde (GA) in 0.1 M phosphate buffer (pH 7.4) (PB) at 4 °C, washed with PB, and postfixed with 2% osmium tetroxide for 90 minutes at RT. After washing with PB, the tissues were dehydrated by a series of ascending ethanol solutions (30, 50, 70, 90 and 2 x 100%) for 10, 10, 10, 30, 30 and 30 minutes. Dehydrated tissues were immersed in t-butyl alcohol for 30 minutes and freeze-dried with EIKO ID-

2. The dried samples were cracked with a razor blade to expose the photoreceptor layer and mounted on the aluminium sample stage. The sample surface was coated with osmium using HPC-1SW (Vacuum device). Then, the samples were analysed with a Hitachi S-4800 scanning electron microscope.

Transmission electron microscopy

For transmission electron microscopy (Habuta et al. 2020), the dissected eyes were fixed overnight in 2% PFA and 2% GA in 0.1 M cacodylate buffer at 4 °C, washed, and postfixed with 2% osmium tetroxide for 90 minutes at RT. After dehydration in an ascending series of ethanol, the samples were embedded in resin. Ultrathin sections (80 nm) were cut with an ultramicrotome Reichert UltraCut S, stained with 2% uranyl acetate and lead solution, and examined with a Hitachi H7650 transmission electron microscope.

Visual motor response of larval fish

Locomotor activity in response to light-dark conditions, also known as visual motor response (VMR), was analysed using the DIY behaviour trace system constructed according to Zhou et al. (2014). Collected eggs were incubated in dechlorinated tap water supplemented with 0.5 mg/L methylene blue at 27 ± 1 °C. Dead eggs were discarded daily. Behavioural tests were carried out at 1 or 2 dph. Larvae were transferred to a 48-well plate filled with 300 µl dechlorinated tap water. LED arrays for white light illumination and infrared LEDs for video recording were placed below the plate. The images were acquired using an industrial monochromatic camera (IDS, UI-3060CP-M-GL Rev.2) placed above the plate and ImageJ with the HF_IDS_Cam plugin (Pasqualin et al. 2018). Only infrared light was recorded by cutting visible wavelength light through a longpass filter (Fujifilm, IR86). The protocol consisted of alternating periods of 30 minutes dark and 30 minutes bright light (3500 ± 360 lux) in a total of 5 cycles. Videos were recorded for 45 sec before and 90 sec after the change in light conditions. Data analysis was performed using ImageJ (Schneider et al. 2012). After subtraction of background and binarization of images, locomotion of larvae was tracked by the wrMTrck plugin (Nussbaum-Krammer et al. 2015). Statistical analysis of the locomotor activities of medaka larva was performed according to the method applied to zebrafish VMR (Liu et al. 2015).

In situ hybridization

In situ hybridization for *bcl2*, *bax, mlkl* and *gabarap* was performed according to the protocol described by Sato et al., 2021.

Statistical analysis

Statistical analyses were performed using Igor Pro 9.00 64-bit (WaveMetrics).

Acknowledgements

We thank all members of our lab for critical comments on this study and Prof. Satoru Miyaishi for permitting us to use his DNA sequencing facility. Confocal microscopy and electron microscopy were performed using facilities of Central Research Laboratory, Okayama University Medical School.

Author contributions

Conceptualization: K.S., H.O.; Methodology: K.S., Y.L.; Formal analysis: K.S.; Investigation: K.S., Y.L., T.Y.; Resources: T.Y.; Data Curation: K.S., H.O.; Writing - Original Draft: K.S., H.O.; Writing - Review & Editing: K.S., T.Y., H.O.; Visualization: K.S.; Supervision: H.O.; Project administration: H.O.; Funding acquisition: K.S., T.Y., H.O.

Compliance and Ethical Standards

Conflict of Interests On behalf of all authors, the corresponding author states that there is no conflict of interest.

Funding

This work was supported by a Grant-in-Aid for Scientific Research to K.S (20K08885), to H.O. (20K21655), a grant from the Takeda Science Foundation to T.Y., grants from the Okayama Medical Foundation and the Takeda Science Foundation to K.T., and a grant from the Astellas Pharma Inc. Research Support to H.O.

Ethical Approval

Not Applicable

Informed Consent

Not Applicable

Supplementary Information

Available online

References

Abd El-Aziz MM, Barragan I, O'Driscoll CA, Goodstadt L, Prigmore E, Borrego S, Mena M, Pieras JI, El-Ashry MF, Safieh LA, Shah A, Cheetham ME, Carter NP, Chakarova C, Ponting CP, Bhattacharya SS, Antinolo G (2008) EYS, encoding an ortholog of Drosophila spacemaker, is mutated in autosomal recessive retinitis pigmentosa. Nat Genet 40:1285–1287. https://doi.org/10.1038/ng.241

Arai Y, Maeda A, Hirami Y, Ishigami C, Kosugi S, Mandai M, Kurimoto Y, Takahashi M (2015) Retinitis Pigmentosa with EYS Mutations Is the Most Prevalent Inherited Retinal Dystrophy in Japanese Populations. J Ophthalmol 2015:819760. https://doi.org/10.1155/2015/819760

Audo I, Sahel J-A, Mohand-Saïd S, Lancelot M-E, Antonio A, Moskova-Doumanova V, Nandrot EF, Doumanov J, Barragan I, Antinolo G, Bhattacharya SS, Zeitz C (2010) EYS is a major gene for rod-cone dystrophies in France. Hum Mutat 31:E1406-1435. https://doi.org/10.1002/humu.21249

Bandah-Rozenfeld D, Littink KW, Ben-Yosef T, Strom TM, Chowers I, Collin RWJ, den Hollander AI, van den Born LI, Zonneveld MN, Merin S, Banin E, Cremers FPM, Sharon D (2010) Novel null mutations in the EYS gene are a frequent cause of autosomal recessive retinitis pigmentosa in the Israeli population. Invest Ophthalmol Vis Sci 51:4387–4394. https://doi.org/10.1167/iovs.09-4732

Barnes CL, Malhotra H, Calvert PD (2021) Compartmentalization of Photoreceptor Sensory Cilia. Front Cell Dev Biol 9:636737. https://doi.org/10.3389/fcell.2021.636737

Brown PK, Gibbons IR, Wald G (1963) THE VISUAL CELLS AND VISUAL PIGMENT OF THE MUDPUPPY, NECTURUS. J Cell Biol 19:79–106. https://doi.org/10.1083/jcb.19.1.79

Carr BJ, Stanar P, Moritz OL (2021) Distinct roles for prominin-1 and photoreceptor cadherin in outer segment disc morphogenesis in CRISPR-altered X. laevis. J Cell Sci 134:jcs253906. https://doi.org/10.1242/jcs.253906

Carter SP, Moran AL, Matallanas D, McManus GJ, Blacque OE, Kennedy BN (2020) Genetic Deletion of Zebrafish Rab28 Causes Defective Outer Segment Shedding, but Not Retinal Degeneration. Front Cell Dev Biol 8

Chen Y, Sawada O, Kohno H, Le Y-Z, Subauste C, Maeda T, Maeda A (2013) Autophagy protects the retina from light-induced degeneration. J Biol Chem 288:7506–7518. https://doi.org/10.1074/jbc.M112.439935

Collin RWJ, Littink KW, Klevering BJ, van den Born LI, Koenekoop RK, Zonneveld MN, Blokland EAW, Strom TM, Hoyng CB, den Hollander AI, Cremers FPM (2008) Identification of a 2 Mb human ortholog of Drosophila eyes shut/spacemaker that is mutated in patients with retinitis pigmentosa. Am J Hum Genet 83:594–603. https://doi.org/10.1016/j.ajhg.2008.10.014

Corral-Serrano JC, Lamers IJC, van Reeuwijk J, Duijkers L, Hoogendoorn ADM, Yildirim A, Argyrou N, Ruigrok RAA, Letteboer SJF, Butcher R, van Essen MD, Sakami S, van Beersum SEC, Palczewski K, Cheetham ME, Liu Q, Boldt K, Wolfrum U, Ueffing M, Garanto A, Roepman R, Collin RWJ (2020) PCARE and WASF3 regulate ciliary F-actin assembly that is required for the initiation of photoreceptor outer segment disk formation. Proc Natl Acad Sci U S A 117:9922–9931. https://doi.org/10.1073/pnas.1903125117

Di Y, Huang L, Sundaresan P, Li S, Kim R, Ballav Saikia B, Qu C, Zhu X, Zhou Y, Jiang Z, Zhang L, Lin Y, Zhang D, Li Y, Zhang H, Yin Y, Lu F, Zhu X, Yang Z (2016) Whole-exome Sequencing Analysis Identifies Mutations in the EYS Gene in Retinitis Pigmentosa in the Indian Population. Sci Rep 6:19432. https://doi.org/10.1038/srep19432

Emran F, Rihel J, Dowling JE (2008) A behavioral assay to measure responsiveness of zebrafish to changes in light intensities. J Vis Exp JoVE 923. https://doi.org/10.3791/923

Fernandes AM, Fero K, Arrenberg AB, Bergeron SA, Driever W, Burgess HA (2012) Deep brain photoreceptors control light-seeking behavior in zebrafish larvae. Curr Biol 22:2042–2047. https://doi.org/10.1016/j.cub.2012.08.016

Fimbel SM, Montgomery JE, Burket CT, Hyde DR (2007) Regeneration of inner retinal neurons after intravitreal injection of ouabain in zebrafish. J Neurosci Off J Soc Neurosci 27:1712–1724. https://doi.org/10.1523/JNEUROSCI.5317-06.2007

Ganzen L, Venkatraman P, Pang CP, Leung YF, Zhang M (2017) Utilizing zebrafish visual behaviors in drug screening for retinal degeneration. Int J Mol Sci 18. https://doi.org/10.3390/ijms18061185

Goldberg AFX, Moritz OL, Williams DS (2016) Molecular basis for photoreceptor outer segment architecture. Prog Retin Eye Res 55:52–81. https://doi.org/10.1016/j.preteyeres.2016.05.003

Habuta M, Fujita H, Sato K, Bando T, Inoue J, Kondo Y, Miyaishi S, Kumon H, Ohuchi H (2020) Dickkopf3 (Dkk3) is required for maintaining the integrity of secretory vesicles in the mouse adrenal medulla. Cell Tissue Res 379:157–167. https://doi.org/10.1007/s00441-019-03113-8

Haltom AR, Lee TV, Harvey BM, Leonardi J, Chen Y-J, Hong Y, Haltiwanger RS, Jafar-Nejad H (2014) The protein O-glucosyltransferase Rumi modifies eyes shut to promote rhabdomere separation in Drosophila. PLoS Genet 10:e1004795. https://doi.org/10.1371/journal.pgen.1004795

Han Z, Anderson DW, Papermaster DS (2012) Prominin-1 localizes to the open rims of outer segment lamellae in Xenopus laevis rod and cone photoreceptors. Invest Ophthalmol Vis Sci 53:361–373. https://doi.org/10.1167/iovs.11-8635

He C, Bartholomew CR, Zhou W, Klionsky DJ (2009) Assaying autophagic activity in transgenic GFP-Lc3 and GFP-Gabarap zebrafish embryos. Autophagy 5:520–526. https://doi.org/10.4161/auto.5.4.7768

Hodel C, Niklaus S, Heidemann M, Klooster J, Kamermans M, Biehlmaier O, Gesemann M, Neuhauss SCF (2014) Myosin VIIA is a Marker for the Cone Accessory Outer Segment in Zebrafish. Anat Rec 297:1777–1784. https://doi.org/10.1002/ar.22976

Hosono K, Ishigami C, Takahashi M, Park DH, Hirami Y, Nakanishi H, Ueno S, Yokoi T, Hikoya A, Fujita T, Zhao Y, Nishina S, Shin JP, Kim IT, Yamamoto S, Azuma N, Terasaki H, Sato M, Kondo M, Minoshima S, Hotta Y (2012) Two novel mutations in the EYS gene are possible major causes of autosomal recessive retinitis pigmentosa in the Japanese population. PloS One 7:e31036. https://doi.org/10.1371/journal.pone.0031036

Hsu Y-C, Chuang J-Z, Sung C-H (2015) Light regulates the ciliary protein transport and outer segment disc renewal of mammalian photoreceptors. Dev Cell 32:731–742. https://doi.org/10.1016/j.devcel.2015.01.027

Huang Y, Zhang J, Li C, Yang G, Liu M, Wang QK, Tang Z (2010) Identification of a novel homozygous nonsense mutation in EYS in a Chinese family with autosomal recessive retinitis pigmentosa. BMC Med Genet 11:121. https://doi.org/10.1186/1471-2350-11-121

Husain N, Pellikka M, Hong H, Klimentova T, Choe K-M, Clandinin TR, Tepass U (2006) The agrin/perlecan-related protein eyes shut is essential for epithelial lumen formation in the Drosophila retina. Dev Cell 11:483–493. https://doi.org/10.1016/j.devcel.2006.08.012

Iwanami M, Oshikawa M, Nishida T, Nakadomari S, Kato S (2012) High prevalence of mutations in the EYS gene in Japanese patients with autosomal recessive retinitis pigmentosa. Invest Ophthalmol Vis Sci 53:1033–1040. https://doi.org/10.1167/iovs.11-9048

Kabeya Y, Mizushima N, Yamamoto A, Oshitani-Okamoto S, Ohsumi Y, Yoshimori T (2004) LC3, GABARAP and GATE16 localize to autophagosomal membrane depending on form-II formation. J Cell Sci 117:2805–2812. https://doi.org/10.1242/jcs.01131

Katagiri S, Akahori M, Hayashi T, Yoshitake K, Gekka T, Ikeo K, Tsuneoka H, Iwata T (2014) Autosomal recessive cone-rod dystrophy associated with compound heterozygous mutations in the EYS gene. Doc Ophthalmol Adv Ophthalmol 128:211–217. https://doi.org/10.1007/s10633-014-9435-0

Khaliq S, Hameed A, Ismail M, Mehdi SQ, Bessant DA, Payne AM, Bhattacharya SS (1999) Refinement of the locus for autosomal recessive Retinitis pigmentosa (RP25) linked to chromosome 6q in a family of Pakistani origin. Am J Hum Genet 65:571–574. https://doi.org/10.1086/302493

Korytowski W, Sarna T (1990) Bleaching of melanin pigments. Role of copper ions and hydrogen peroxide in autooxidation and photooxidation of synthetic dopa-melanin. J Biol Chem 265:12410–12416. https://doi.org/10.1016/S0021-9258(19)38362-0

Kusmic C, Barsanti L, Passarelli V, Gualtieri P (1993) Photoreceptor morphology and visual pigment content in the pineal organ and in the retina of juvenile and adult trout, Salmo irideus. Micron 24:279–286. https://doi.org/10.1016/0968-4328(93)90054-5

Larhammar D, Nordström K, Larsson TA (2009) Evolution of vertebrate rod and cone phototransduction genes. Philos Trans R Soc Lond B Biol Sci 364:2867-80. https://doi.org/10.1098/rstb.2009.0077

Liu Y, Carmer R, Zhang G, Venkatraman P, Brown SA, Pang C-P, Zhang M, Ma P, Leung YF (2015) Statistical Analysis of Zebrafish Locomotor Response. PloS One 10:e0139521. https://doi.org/10.1371/journal.pone.0139521

Lu Z, Hu X, Liu F, Soares DC, Liu X, Yu S, Gao M, Han S, Qin Y, Li C, Jiang T, Luo D, Guo A-Y, Tang Z, Liu M (2017) Ablation of EYS in zebrafish causes mislocalisation of outer segment proteins, F-actin disruption and cone-rod dystrophy. Sci Rep 7:46098. https://doi.org/10.1038/srep46098

Lu Z, Hu X, Reilly J, Jia D, Liu F, Yu S, Liu X, Xie S, Qu Z, Qin Y, Huang Y, Lv Y, Li J, Gao P, Wong F, Shu X, Tang Z, Liu M (2019) Deletion of the transmembrane protein Prom1b in zebrafish disrupts outer-segment morphogenesis and causes photoreceptor degeneration. J Biol Chem 294:13953–13963. https://doi.org/10.1074/jbc.RA119.008618

Lust K, Wittbrodt J (2018) Activating the regenerative potential of Müller glia cells in a regeneration-deficient retina. eLife 7:e32319. https://doi.org/10.7554/eLife.32319

Messchaert M, Dona M, Broekman S, Peters TA, Corral-Serrano JC, Slijkerman RWN, van Wijk E, Collin RWJ (2018) Eyes shut homolog is important for the maintenance of photoreceptor morphology and visual function in zebrafish. PloS One 13:e0200789. https://doi.org/10.1371/journal.pone.0200789

Naito Y, Hino K, Bono H, Ui-Tei K (2015) CRISPRdirect: software for designing CRISPR/Cas guide RNA with reduced off-target sites. Bioinformatics 31:1120–1123. https://doi.org/10.1093/bioinformatics/btu743

Nakamura S, Akayama S, Yoshimori T (2022) Non-canonical roles of ATG8 for TFEB activation. Biochem Soc Trans 50:47–54. https://doi.org/10.1042/BST20210813

Nakamura S, Yoshimori T (2017) New insights into autophagosome-lysosome fusion. J Cell Sci 130:1209–1216. https://doi.org/10.1242/jcs.196352

Newton F, Megaw R (2020) Mechanisms of Photoreceptor Death in Retinitis Pigmentosa. Genes 11:E1120. https://doi.org/10.3390/genes11101120

Nie J, Mahato S, Mustill W, Tipping C, Bhattacharya SS, Zelhof AC (2012) Cross species analysis of Prominin reveals a conserved cellular role in invertebrate and vertebrate photoreceptor cells. Dev Biol 371:312–320. https://doi.org/10.1016/j.ydbio.2012.08.024

Nishiguchi KM, Miya F, Mori Y, Fujita K, Akiyama M, Kamatani T, Koyanagi Y, Sato K, Takigawa T, Ueno S, Tsugita M, Kunikata H, Cisarova K, Nishino J, Murakami A, Abe T, Momozawa Y, Terasaki H, Wada Y, Sonoda K-H, Rivolta C, Tsunoda T, Tsujikawa M, Ikeda Y, Nakazawa T (2021) A hypomorphic variant in EYS detected by genome-wide association study contributes toward retinitis pigmentosa. Commun Biol 4:140. https://doi.org/10.1038/s42003-021-01662-9

Numa S, Oishi A, Higasa K, Oishi M, Miyata M, Hasegawa T, Ikeda HO, Otsuka Y, Matsuda F, Tsujikawa A (2020) EYS is a major gene involved in retinitis pigmentosa in Japan: genetic landscapes revealed by stepwise genetic screening. Sci Rep 10:20770. https://doi.org/10.1038/s41598-020-77558-1

Nussbaum-Krammer CI, Neto MF, Brielmann RM, Pedersen JS, Morimoto RI (2015) Investigating the Spreading and Toxicity of Prion-like Proteins Using the Metazoan Model Organism C.

elegans. JoVE J Vis Exp e52321. https://doi.org/10.3791/52321

O'Neal TB, Luther EE (2021) Retinitis Pigmentosa. In: StatPearls. StatPearls Publishing, Treasure Island (FL)

Pasqualin C, Gannier F, Bredeloux P, Maupoil V (2018) HF_IDS_Cam: Fast Video Capture with ImageJ for Real-Time Analysis. J Imaging 4:44. https://doi.org/10.3390/jimaging4020044

Pierrache LHM, Messchaert M, Thiadens AAHJ, Haer-Wigman L, de Jong-Hesse Y, van Zelst-Stams WAG, Collin RWJ, Klaver CCW, van den Born LI (2019) Extending the Spectrum of EYS-Associated Retinal Disease to Macular Dystrophy. Invest Ophthalmol Vis Sci 60:2049–2063. https://doi.org/10.1167/iovs.18-25531

Ruiz A, Borrego S, Marcos I, Antiñolo G (1998) A major locus for autosomal recessive retinitis pigmentosa on 6q, determined by homozygosity mapping of chromosomal regions that contain gamma-aminobutyric acid-receptor clusters. Am J Hum Genet 62:1452–1459. https://doi.org/10.1086/301866

Sahly I, Dufour E, Schietroma C, Michel V, Bahloul A, Perfettini I, Pepermans E, Estivalet A, Carette D, Aghaie A, Ebermann I, Lelli A, Iribarne M, Hardelin J-P, Weil D, Sahel J-A, El-Amraoui A, Petit C (2012) Localization of Usher 1 proteins to the photoreceptor calyceal processes, which are absent from mice. J Cell Biol 199:381–399. https://doi.org/10.1083/jcb.201202012

Sato K, Khine Nwe Nwe, Ohuchi H (2021) The Opsin 3/Teleost multiple tissue opsin system: mRNA localization in the retina and brain of medaka (Oryzias latipes). J Comp Neurol 529:2484–2516. https://doi.org/10.1002/cne.25106

Sato K, Yamashita T, Haruki Y, Ohuchi H, Kinoshita M, Shichida Y (2016) Two UV-sensitive photoreceptor proteins, Opn5m and Opn5m2 in ray-finned fish with distinct molecular properties and broad distribution in the retina and brain. PloS One 11:e0155339. https://doi.org/10.1371/journal.pone.0155339

Schaaf MBE, Keulers TG, Vooijs MA, Rouschop KMA (2016) LC3/GABARAP family proteins: autophagy-(un)related functions. FASEB J Off Publ Fed Am Soc Exp Biol 30:3961–3978. https://doi.org/10.1096/fj.201600698R

Schartl M, Walter RB, Shen Y, Garcia T, Catchen J, Amores A, Braasch I, Chalopin D, Volff J-N, Lesch K-P, Bisazza A, Minx P, Hillier L, Wilson RK, Fuerstenberg S, Boore J, Searle S, Postlethwait JH, Warren WC (2013) The genome of the platyfish, Xiphophorus maculatus,

provides insights into evolutionary adaptation and several complex traits. Nat Genet 45:567–572. https://doi.org/10.1038/ng.2604

Schietroma C, Parain K, Estivalet A, Aghaie A, Boutet de Monvel J, Picaud S, Sahel J-A, Perron M, El-Amraoui A, Petit C (2017) Usher syndrome type 1-associated cadherins shape the photoreceptor outer segment. J Cell Biol 216:1849–1864. https://doi.org/10.1083/jcb.201612030

Schneider CA, Rasband WS, Eliceiri KW (2012) NIH Image to ImageJ: 25 years of Image Analysis. Nat Methods 9:671–675

Shi X, Garcia G, Van De Weghe JC, McGorty R, Pazour GJ, Doherty D, Huang B, Reiter JF (2017) Super-resolution microscopy reveals that disruption of ciliary transition-zone architecture causes Joubert syndrome. Nat Cell Biol 19:1178–1188. https://doi.org/10.1038/ncb3599

Spencer WJ, Lewis TR, Phan S, Cady MA, Serebrovskaya EO, Schneider NF, Kim K-Y, Cameron LA, Skiba NP, Ellisman MH, Arshavsky VY (2019) Photoreceptor disc membranes are formed through an Arp2/3-dependent lamellipodium-like mechanism. Proc Natl Acad Sci U S A 201913518. https://doi.org/10.1073/pnas.1913518117

Takita S, Seko Y (2020) eys +/- ; lrp5 +/- Zebrafish Reveals Lrp5 Can Be the Receptor of Retinol in the Visual Cycle. iScience 23:101762. https://doi.org/10.1016/j.isci.2020.101762

Tang Z, Lin MG, Stowe TR, Chen S, Zhu M, Stearns T, Franco B, Zhong Q (2013) Autophagy promotes primary ciliogenesis by removing OFD1 from centriolar satellites. Nature 502:254–257. https://doi.org/10.1038/nature12606

Verbakel SK, van Huet RAC, Boon CJF, den Hollander AI, Collin RWJ, Klaver CCW, Hoyng CB, Roepman R, Klevering BJ (2018) Non-syndromic retinitis pigmentosa. Prog Retin Eye Res 66:157–186. https://doi.org/10.1016/j.preteyeres.2018.03.005

Verschueren A, Boucherit L, Ferrari U, Fouquet S, Nouvel-Jaillard C, Paques M, Picaud S, Sahel J-A (2022) Planar polarity in primate cone photoreceptors: a potential role in Stiles Crawford effect phototropism. Commun Biol 5:1–13. https://doi.org/10.1038/s42003-021-02998-y

Weigmann A, Corbeil D, Hellwig A, Huttner WB (1997) Prominin, a novel microvilli-specific polytopic membrane protein of the apical surface of epithelial cells, is targeted to plasmalemmal protrusions of non-epithelial cells. Proc Natl Acad Sci 94:12425−12430. https://doi.org/10.1073/pnas.94.23.12425

Wen RH, Stanar P, Tam B, Moritz OL (2019) Autophagy in Xenopus laevis rod photoreceptors is independently regulated by phototransduction and misfolded RHOP23H. Autophagy 15:1970–1989. https://doi.org/10.1080/15548627.2019.1596487

Westin IM, Jonsson F, Österman L, Holmberg M, Burstedt M, Golovleva I (2021) EYS mutations and implementation of minigene assay for variant classification in EYS-associated retinitis pigmentosa in northern Sweden. Sci Rep 11:7696. https://doi.org/10.1038/s41598-021-87224-9

Wittbrodt J, Shima A, Schartl M (2002) Medaka--a model organism from the far East. Nat Rev Genet 3:53–64. https://doi.org/10.1038/nrg704

Wright AF, Chakarova CF, Abd El-Aziz MM, Bhattacharya SS (2010) Photoreceptor degeneration: genetic and mechanistic dissection of a complex trait. Nat Rev Genet 11:273–284. https://doi.org/10.1038/nrg2717

Yamamoto Y, Chino H, Tsukamoto S, Ode KL, Ueda HR, Mizushima N (2021) NEK9 regulates primary cilia formation by acting as a selective autophagy adaptor for MYH9/myosin IIA. Nat Commun 12:3292. https://doi.org/10.1038/s41467-021-23599-7

Yamamoto Y, Mizushima N (2021) Autophagy and Ciliogenesis. JMA J 4:207–215. https://doi.org/10.31662/jmaj.2021-0090

Yang L, Fujinami K, Ueno S, Kuniyoshi K, Hayashi T, Kondo M, Mizota A, Naoi N, Shinoda K, Kameya S, Fujinami-Yokokawa Y, Liu X, Arno G, Pontikos N, Kominami T, Terasaki H, Sakuramoto H, Katagiri S, Mizobuchi K, Nakamura N, Mawatari G, Kurihara T, Tsubota K, Miyake Y, Yoshitake K, Iwata T, Tsunoda K, JEGC study group (2020) Genetic Spectrum of EYS-associated Retinal Disease in a Large Japanese Cohort: Identification of Disease-associated Variants with Relatively High Allele Frequency. Sci Rep 10:5497. https://doi.org/10.1038/s41598-020-62119-3

Yu M, Liu Y, Li J, Natale BN, Cao S, Wang D, Amack JD, Hu H (2016) Eyes shut homolog is required for maintaining the ciliary pocket and survival of photoreceptors in zebrafish. Biol Open 5:1662–1673. https://doi.org/10.1242/bio.021584

Zelhof AC, Hardy RW, Becker A, Zuker CS (2006) Transforming the architecture of compound eyes. Nature 443:696–699. https://doi.org/10.1038/nature05128

Zhang L, Xiang L, Liu Y, Venkatraman P, Chong L, Cho J, Bonilla S, Jin ZB, Pang CP, Ko KM, Ma

P, Zhang M, Leung YF. (2016) A Naturally-Derived Compound Schisandrin B Enhanced Light Sensation in the pde6c Zebrafish Model of Retinal Degeneration. PLoS One 11:e0149663. doi: 10.1371/journal.pone.0149663.

Zhang R, Oglesby E, Marsh-Armstrong N (2008) Xenopus laevis P23H rhodopsin transgene causes rod photoreceptor degeneration that is more severe in the ventral retina and is modulated by light. Exp Eye Res 86:612–621. https://doi.org/10.1016/j.exer.2008.01.005

Zhou Y, Cattley RT, Cario CL, Bai Q, Burton EA (2014) Quantification of larval zebrafish motor function in multi-well plates using open-source MATLAB® applications. Nat Protoc 9:1533–1548. https://doi.org/10.1038/nprot.2014.094

Figures

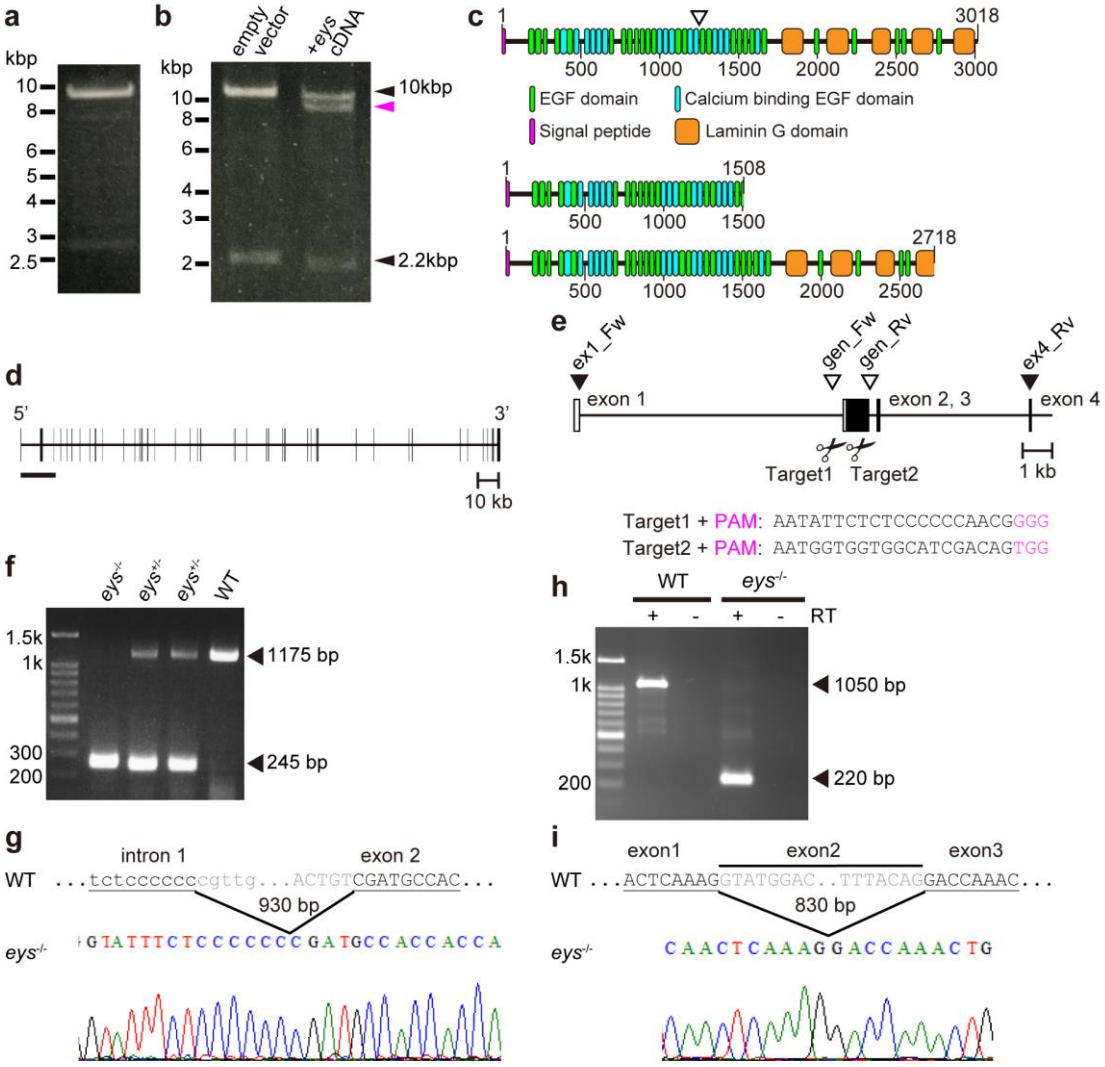

Fig. 1 Identification of full-length medaka *eys* transcript and generation of *eys* knockout medaka. **a** Amplification and isolation of the full-length coding region of medaka *eys* cDNA. A single DNA band was detected at the expected size (9 kbp) by agarose gel electrophoresis after RT–PCR, nested PCR and NotI digestion. **b** Representative plasmid clone with or without insertion of *eys* cDNA. Plasmids were electrophoresed after digestion by NotI. Black arrowheads indicate the size of the digested fragment of the pJAZZ OC vector. The magenta arrowhead indicates the position of inserted *eys* cDNA. **c** Domain structure of medaka EYS protein. Medaka EYS is predicted to consist of the N-terminal signal peptide, 41 EGF-like domains and five laminin G domains. The open triangle indicates the position of the sequence homologous to the epitope of the anti-EYS antibody (EYS/RP25 Antibody, Novus Biologicals #NBP1-90038) (1239-1305 a.a.). Among three fully sequenced clones, one corresponds to the full sequence of medaka *eys*

(upper one). The amino acid sequences of the remaining two clones are truncated at premature stop codons that appear due to internal deletions or insertions (lower two). **d** Gene structure of medaka *eys*. Black boxes and black lines between boxes indicate exons and introns, respectively. The medaka *eys* gene comprises 51 exons. The thick black bar under the 5' region indicates the region containing exons 1-4 enlarged in Panel **e**. **e** Targeted positions by Cas9 guide RNAs. Open and filled boxes indicate untranslated and coding regions in exons, respectively. The targeted sequence positions of guide RNAs are indicated by scissor symbols. Open and filled triangles indicate the positions of primers for genomic PCR shown in Panel C and RT–PCR shown in Panel E, respectively. **f** Representative genomic PCR results of $eys^{-/-}$, $eys^{+/-}$, and wild-type (WT) medaka. **g** Sanger sequencing of the genomic region containing a deletion. In the WT sequence, nucleotides in introns and exons are lettered in lowercase and uppercase letters, respectively. The sequencing result for $eys^{-/-}$ shows deletion of 930 bp over intron 1 and exon 2 indicated by grey letters in WT. **h** Validation of *eys* transcripts by RT–PCR using RNA from eyes of WT and $eys^{-/-}$ medaka. Forward and reverse primers were designed in exons 1 and 4, respectively. **i** Sanger sequencing of the RT–PCR product of $eys^{-/-}$. In the WT sequence, the sequences corresponding to exons 1 and 3 are underlined. The sequencing result for the $eys^{-/-}$ transcript shows a deletion of 830 bp in exon 2, indicated by grey letters for WT

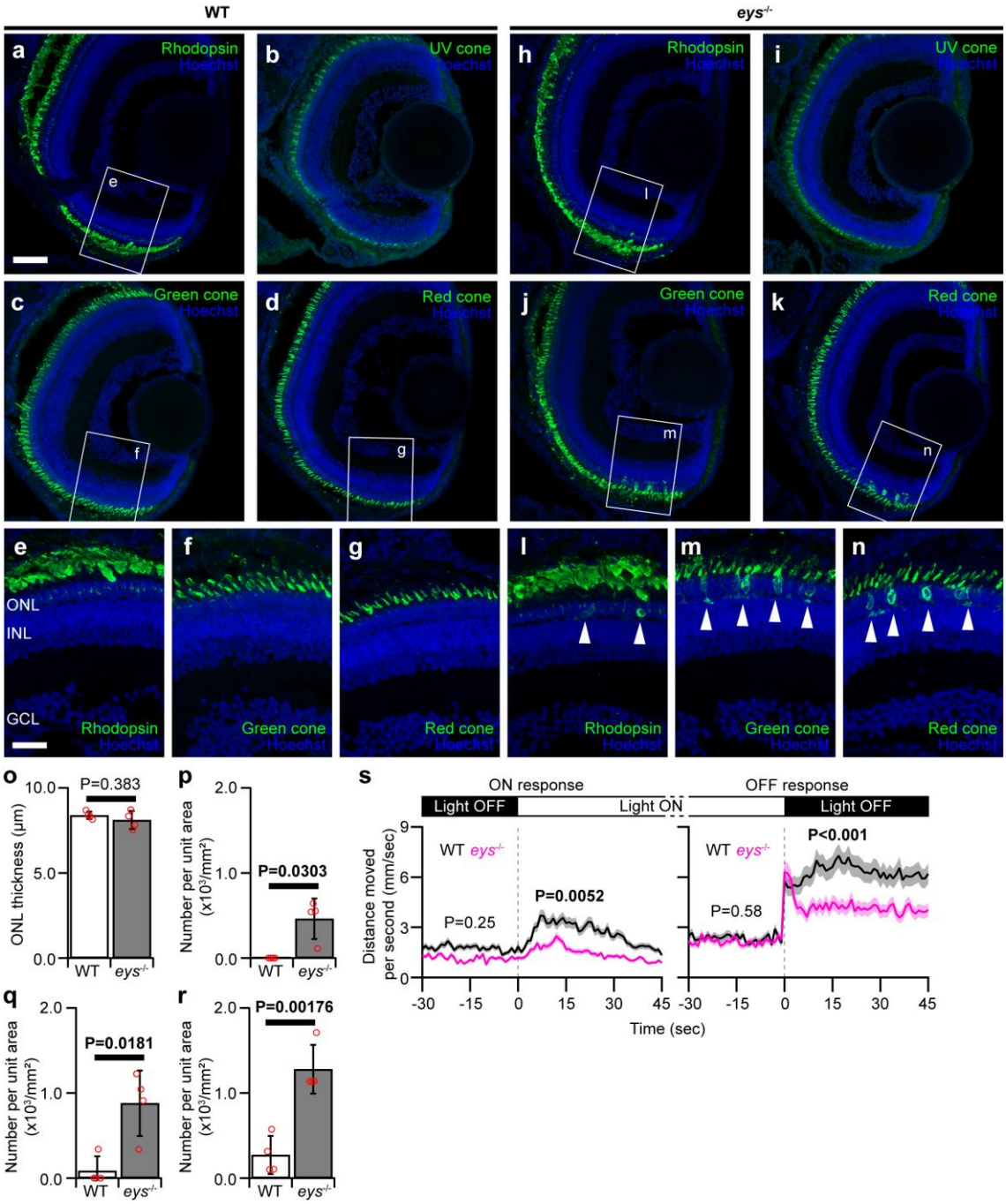

Fig. 2 Abnormalities of photoreceptor organization and response to light in WT and *eys*$^{-/-}$ medaka larvae. **a** Visual motor responses in WT and *eys*$^{-/-}$ medaka. Light-on and light-off visual motor response (VMR) of 1 or 2 dph medaka placed in each well of a 48-well plate. Their behaviour was tracked by turning a white light (~3500 lux) on and off 5 times every 30 minutes. The third record of the light-on and light-off trials is shown as representative. The distance of movement per second was plotted against time for 30 seconds before and 45 seconds after light alteration (t = 0). Solid traces and shadings

indicate the mean ± standard error of the mean (s.e.m.) (n = 84 for WT, n = 80 for *eys*$^{-/-}$). Traces of WT and *eys*$^{-/-}$ medaka are shown in black and magenta, respectively. P values were estimated by Hotelling's T-squared test. **b-s** Immunofluorescence staining with anti-visual pigment (green) antibodies of WT (**b-h**) and *eys*$^{-/-}$ (**i-o**) retinas at 1 dph. Panels **f-h** and **m-o** show enlarged views of the region indicated by rectangles in panels **b**, **d**, **e**, **i**, **k**, and **l**. The arrowheads indicate photoreceptor cells exhibiting mislocalized visual pigments. All sections were counterstained with Hoechst 33342 (blue). All images in this figure are maximum intensity projections of the z-stack. **p** The thickness of ONL in the fundus near the posterior pole. The thickness of ONL was estimated based on the fluorescence of Hoechst 33342. **q-s** The number of photoreceptor cells exhibiting mislocalization of rhodopsin (**q**), green cone pigment (**r**), or red cone pigment (**s**) in the cell body or synaptic terminal. Data in panels **p-s** are shown as the means ± standard deviation (s.d.) (n = 4). P values were calculated by unpaired two-tailed Student's t test. Red open circles indicate values from individual samples. GCL, ganglion cell layer; INL, inner nuclear layer; ONL, outer nuclear layer. Scale bar: 50 μm in **b** for **b-e** and **i-l**; 20 μm in **f** for **f-h** and **m-o**

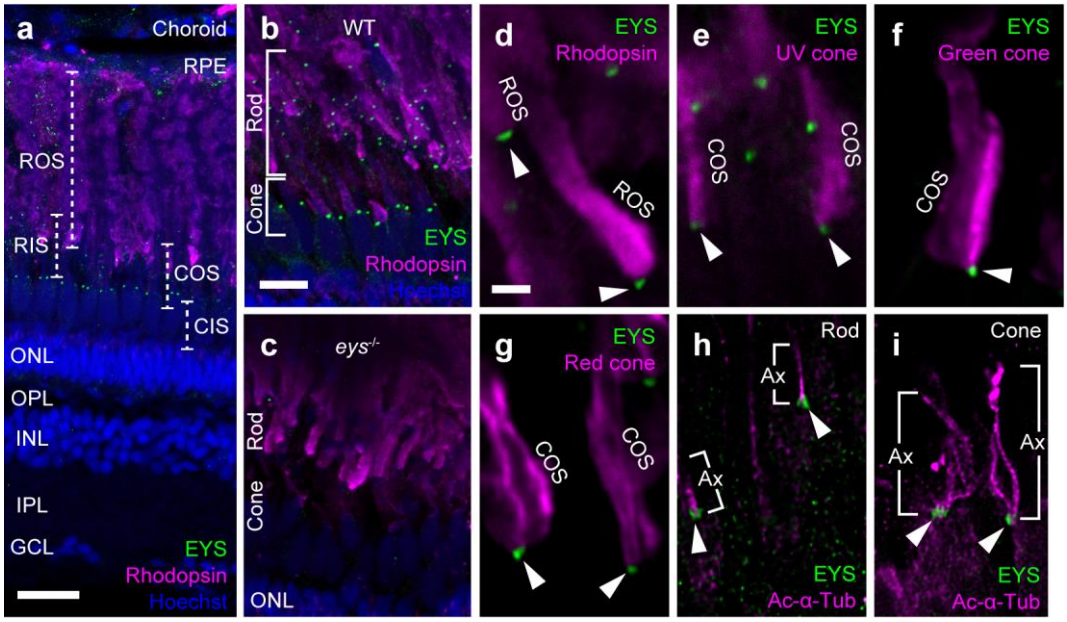

Fig. 3 Immunofluorescent characterization of EYS protein in medaka retina. **a** Overall view of retinal layer structure of the WT adult medaka stained with anti-EYS (green) and anti-rhodopsin (magenta). Dotted lines indicate the rod outer segments (ROS), ellipsoid part of rod inner segments (RIS), cone outer segments (COS), and cone inner segments (CIS) are present, respectively. **b, c** Comparative immunostaining of retinas from WT (**b**) and *eys*$^{-/-}$ (**c**) medaka at 8 mph with anti-EYS (green) and anti-rhodopsin (magenta) antibodies. EYS shows punctate immunoreactivities at the basal region of the rod and cone outer segments in WT. Those immunoreactivities are absent in the *eys*$^{-/-}$ retina. Cell nuclei were counterstained with Hoechst 33342 (blue). **d-i** Double immunofluorescent staining with anti-rhodopsin (**d**), anti-UV cone (**e**), Rho4D2 antibody (staining medaka green cone) (**f**), anti-red cone (**g**), and anti-acetylated α-tubulin (**h, i**) in addition to anti-EYS. The basal regions of the rod and cone are shown in panels **h** and **i**, respectively. Retinas from WT 8-mph medaka were stained. Single optical sections are shown in panels **d-i**. White arrowheads indicate the EYS immunoreactivity. Faint green puncta in panel h that are not indicated by arrowheads are noise. GCL, ganglion cell layer; IPL, inner plexiform layer; INL, inner nuclear layer; OPL, outer plexiform layer; ONL, outer nuclear layer; RPE, retinal pigment epithelium. Scale bar: 20 μm in **a**; **b**: 10 μm in **b** for **b** and **c**; 2 μm in **d** for **d-i**

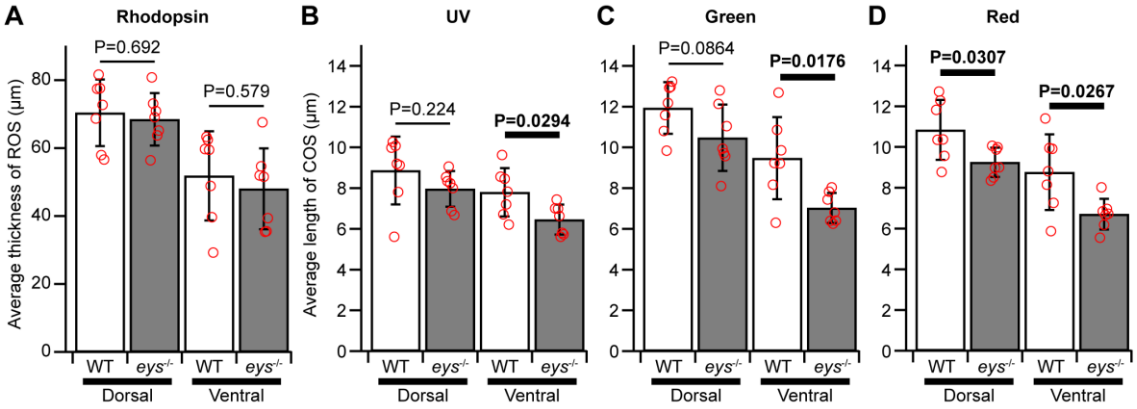

Fig. 4 Outer segment length in WT and *eys*$^{-/-}$ medaka retina. **a** The thickness of the rod outer segment (ROS) layer was estimated based on the rhodopsin immunoreactive region in the retina (Figure S4). **b-d** Averaged lengths of outer segments of UV (**b**), green (**c**), and red (**d**) cone photoreceptors were measured and estimated based on the cone visual pigment immunoreactivities (Fig. S4). All data were obtained from 8-mph medakas. The dorsal to central and ventral to central regions were separately analysed. Data are indicated as the means ± s.d. (n = 7). Red open circles indicate individual values. P values were estimated by the unpaired two-tailed Student's t test

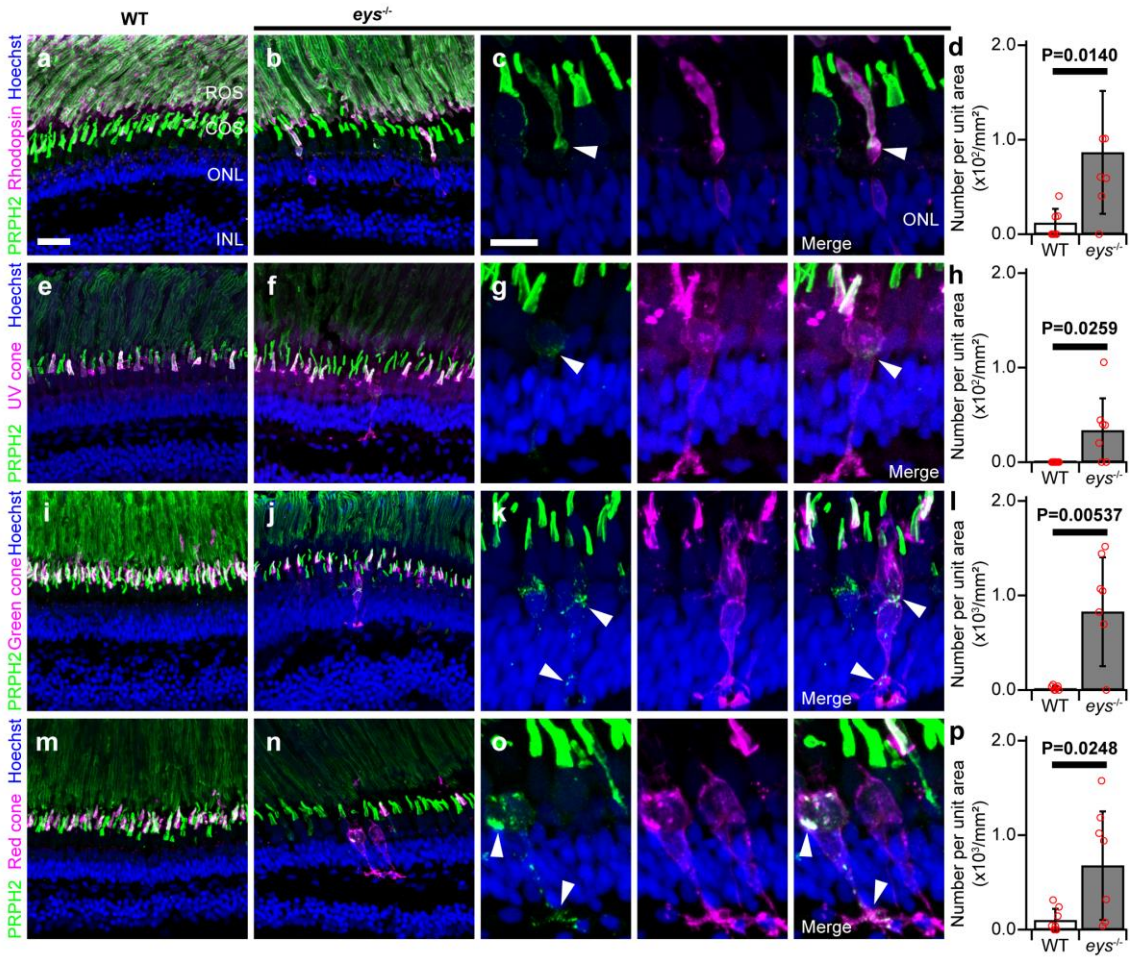

Fig. 5 Mislocalization of outer segment proteins in *eys*$^{-/-}$ medaka retina. **a-c, e-g, i-k, m-o** Double immunofluorescent staining using anti-peripherin2 (green) and anti-visual pigment (magenta) antibodies of WT (**a, e, i, m**) and *eys*$^{-/-}$ (**b, c, f, g, j, k, n, o**) retinas at 8 mph. Panels **c, g, k** and **o** show enlarged views of the photoreceptor cell exhibiting mislocalized peripherin2 and visual pigments. Peripherin2 only (left panels), visual pigment only (centre panels), and the merged view (right panels) are shown. The arrowheads indicate the mislocalized immunoreactivities of peripherin2 alone or with visual pigments. **d, h, l, p** The number of photoreceptor cells exhibiting mislocalized visual pigment immunoreactivity in the cell body or synaptic terminal. Data are shown as the means ± s.d. (n = 7). P values were estimated by unpaired two-tailed Student's t test. Red open circles indicate individual values. Cell counting was performed with anti-rhodopsin (**a-d**), anti-UV cone (**e-h**), Rho4D2 (**i-l**), and anti-red cone antibodies (**m-p**). All sections were counterstained with Hoechst 33342 (blue). All images in this figure are maximum intensity projections of the z-stack. Scale bar: 20 μm in **a** for **a, b, e, f, i, j, m** and **n**; 10 μm in **c** for **c, g, k** and **o**

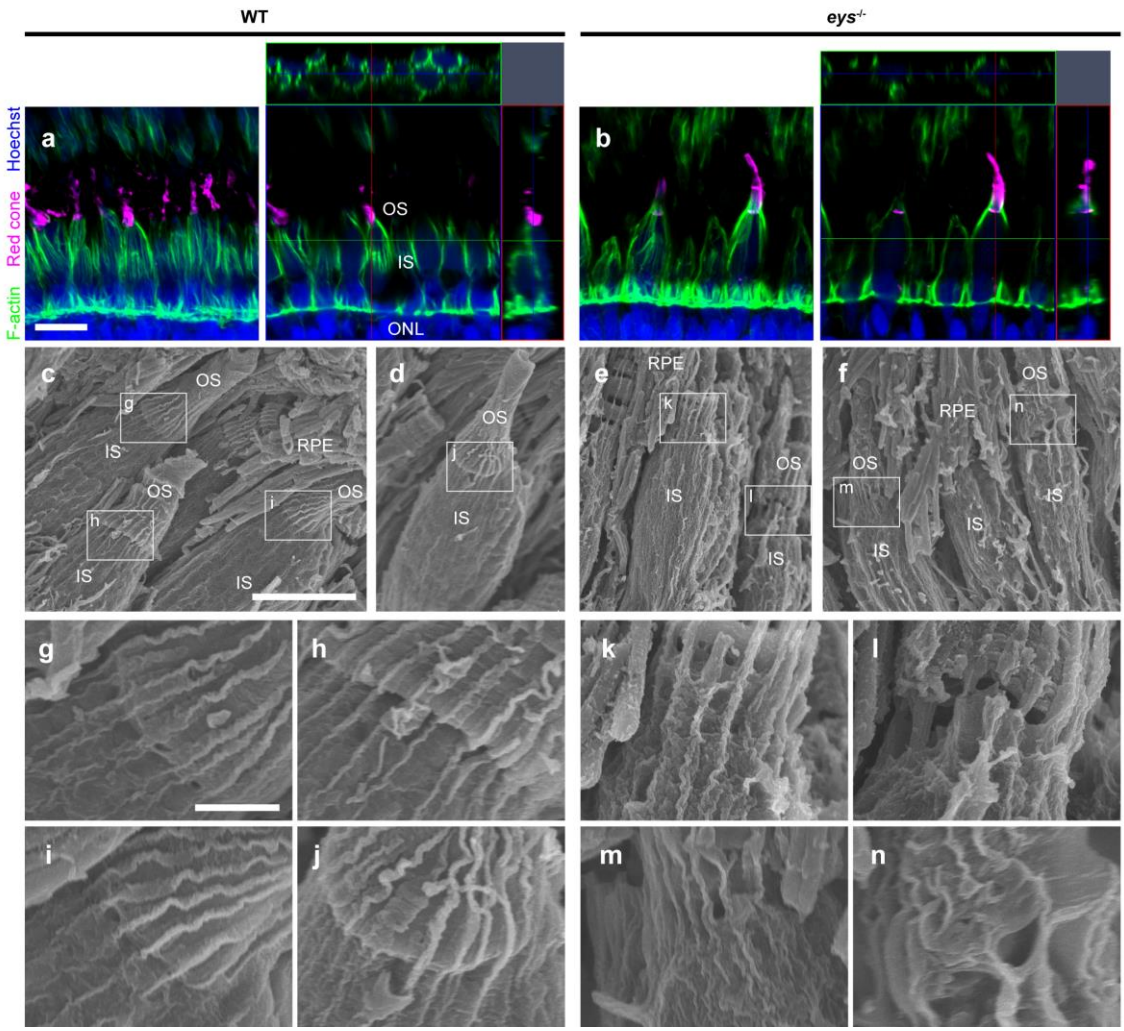

Fig. 6 Disruption of the F-actin arrangement in *eys*$^{-/-}$ medaka retina. **a, b** Fluorescent staining by TRITC-phalloidin (green) and anti-red cone visual pigment antibody (magenta) of WT (**a**) and *eys*$^{-/-}$ (**b**) retinas at 8 mph. The left panels show the maximum intensity projection of the z-stack. The right panels show the single optical section in the blue rectangle with the xz- (in green rectangle) and xy-orthogonal (in red rectangle) projection at the level of green and red lines, respectively. Cell nuclei in panels **a** and **b** were counterstained with Hoechst 33342 (blue). **c-f** Scanning electron microscopy imaging of cone photoreceptors in WT (**c, d**) and *eys*$^{-/-}$ (**e, f**) medaka retinas. IS, inner segment; OS, outer segment; RPE, retinal pigment epithelial cell. Scale bar **a**: 10 μm in **a** for **a** and **b**; 5 μm in **c** for **c-f;** 1 μm in **g** for **g-n**

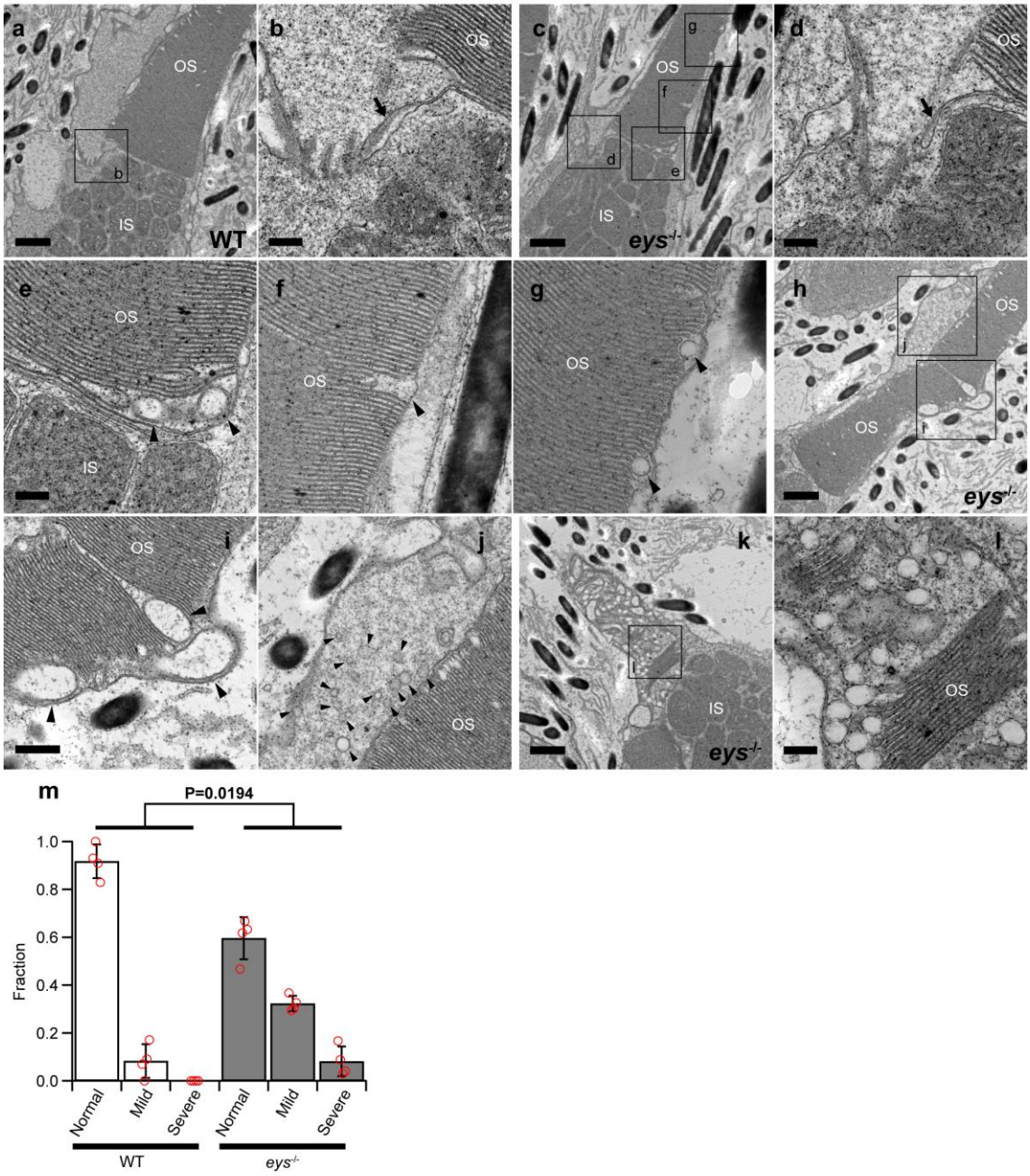

Fig. 7 Ultrastructural analysis of the photoreceptor outer segment in WT and *eys*$^{-/-}$ medaka retinas. **a** Transmission electron microscopy (TEM) imaging of cone photoreceptors of WT medaka. The rectangle indicates the region enlarged in panel **b**. **b** Enlarged view of the region near the connecting cilia. The arrow indicates the ciliary pocket. **c** TEM imaging of cone photoreceptors of *eys*$^{-/-}$ medaka. Rectangles indicate the regions enlarged in panels **d-g**. **d** Enlarged view of the region near the connecting cilia. The arrow indicates the ciliary pocket. **e** Abnormal vesicles in the outer segment of the proximal region (arrowheads). **f** Interrupted lamellar membrane in the outer segment (arrowhead). **g**

Abnormal small vesicles in the outer segment of the distal region (arrowheads). **h** TEM imaging of moderately damaged cone photoreceptors of *eys*$^{-/-}$ medaka. Rectangles indicate the regions enlarged in panels **i** and **j**. **i** Disturbance of the uniform lamellar membrane structure by the abnormal vesicles (arrowheads). **j** Infiltration of the vesicles (arrowheads) into the accessary cone. **k** TEM imaging of severely damaged cone photoreceptors of *eys*$^{-/-}$ medaka. The rectangle indicates the region enlarged in panel **l**. **l** The outer segment of this cone photoreceptor is nearly completely destroyed by the infiltration of abnormal vesicles. Only a small amount of the lamellar structure remains. **m** Based on the region of normal lamellar morphology, photoreceptors were classified into three classes: normal morphology (>97% uniform lamellar structure), mildly damaged (50-97% uniform lamellar structure), and severely damaged (≦50% uniform lamellar structure). Based on the counting of these photoreceptors from four individual fish for WT and *eys* KO, the mean fraction of each class and s.d. were calculated. The P value was estimated by Hotelling's T-squared test. Scale bar: 1 μm in **a, c, h** and **k**; 200 nm in **b, d, e** (for **e-g**) and **l**; 400 nm in **i** for **i** and **j**

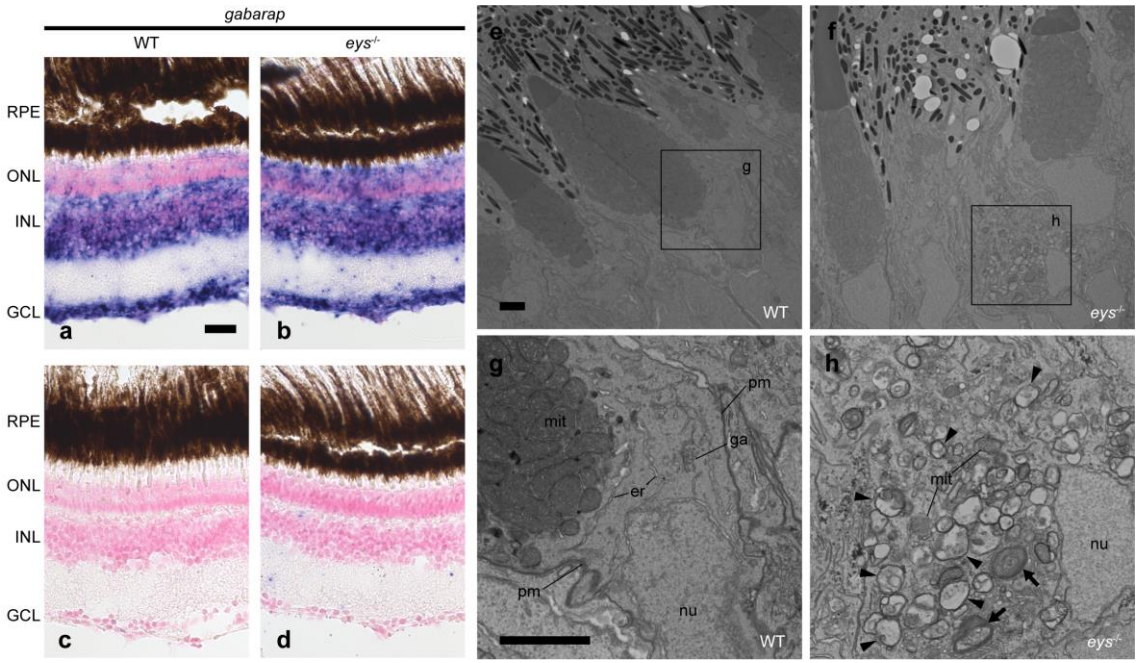

Fig. 8 *eys*-deficient medaka retina shows signs of autophagy. **a-d** The distribution of mRNAs of *gabarap*, a regulator gene for autophagy, in WT (**a, c**) and *eys*$^{-/-}$ (**b, d**) medaka retinas at 4 mph was observed by in situ hybridization. Retinal sections were hybridized with an antisense (**a, b**) or a sense (**c, d**) probe of *gabarap*. The sections in panels **a-d** were counterstained with Nuclear Fast Red. **e-h** TEM imaging of cone photoreceptors in WT (**e, g**) and *eys*$^{-/-}$ (**f, h**) medaka retina. The rectangles indicate the region enlarged in panels **g** and **f**. **g** Enlarged view of the inner segment of a normal cone photoreceptor. **f** Enlarged view of the region showing characteristic features of autophagy. Arrows and arrowheads indicate multilamellar bodies and autophagic vacuoles, respectively. er, endoplasmic reticulum; ga, Golgi apparatus; mit, mitochondrion; nu, nucleus; pm, plasma membrane. Scale bar: 20 μm in **a** for **a-d**; 2 μm in **e (**for **e** and **f)** and in **g** (for **g** and **h**)

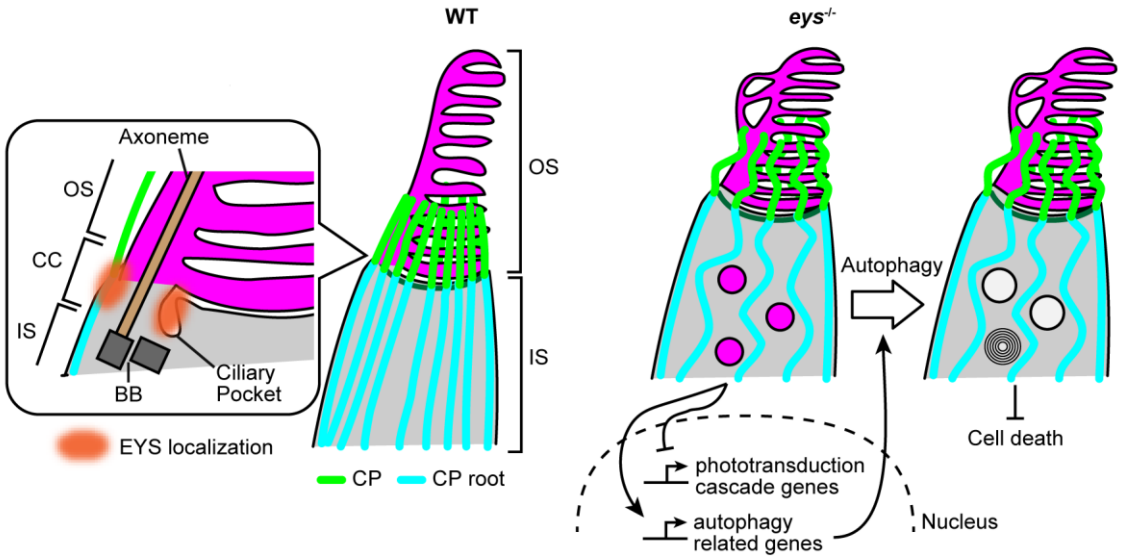

Fig. 9 The effect of genetic ablation of *eys* in medaka photoreceptors is depicted schematically. The balloon in the WT panel represents the region where EYS protein is localized, near the connecting cilia (CC). In *eys*$^{-/-}$ cone photoreceptors, protein transport to the outer segment (OS) is impaired (circles filled in magenta), actin filament networks and calyceal processes (rods in green and aqua blue) are disorganized, and OS morphology is disturbed, leading to reduced expression of phototransduction cascade genes and upregulation of autophagy-related genes. By eliminating OS proteins that have accumulated due to the protein transport defects, autophagy is thought to alleviate cellular stress and prevent cell death. Vacuoles and a multilamellar body, the signs of autophagy, are represented by hollow circles and a concentric circle, respectively. BB, basal body; CP, calyceal process; IS, inner segment.